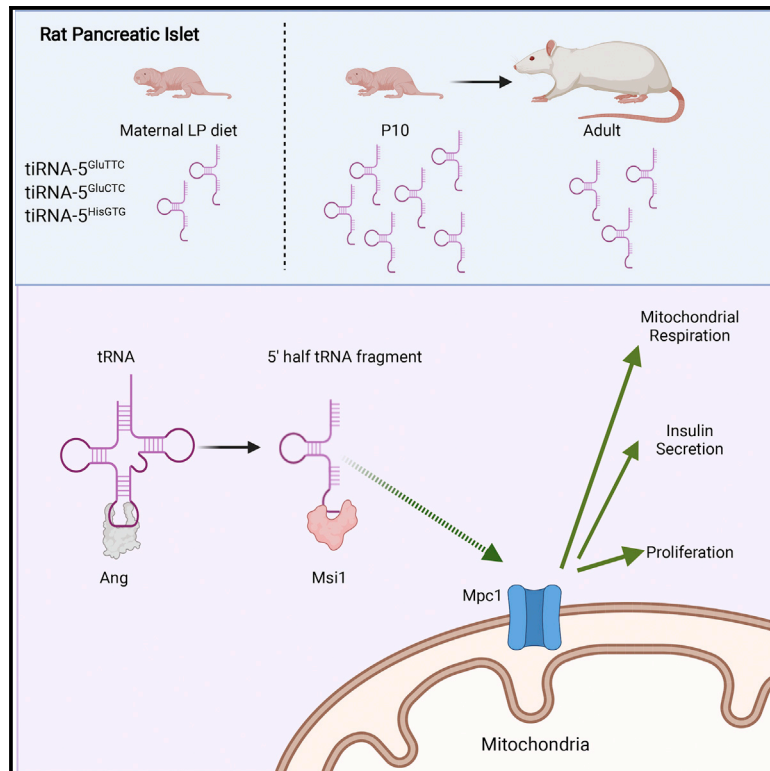


Small RNAs derived from tRNA fragmentation regulate the functional maturation of neonatal β cells

Graphical abstract



Authors

Mustafa Bilal Bayazit, Cécile Jacovetti, Cristina Cosentino, ..., Lisa Stoll, Claudiane Guay, Romano Regazzi

Correspondence

romano.regazzi@unil.ch

In brief

Bayazit et al. report that tRNA halves generated from His and Glu tRNAs (tiRNA-5s) are abundant in the islets of neonatal rats at a critical time point in β cell development. These tRNA fragments are enriched in mitochondrial fractions and contribute to neonatal β cell-mass expansion and insulin secretion.

Highlights

- 5' tRNA halves (tiRNA-5s) are abundant in pancreatic islets of neonatal rats
- tiRNA-5^{HisGTG} and GluCTC are enriched in mitochondrial fractions of β cells
- They control mitochondrial respiration, β cell proliferation, and insulin secretion
- Inappropriate intrauterine conditions reduce the level of these tiRNA-5s



Article

Small RNAs derived from tRNA fragmentation regulate the functional maturation of neonatal β cells

Mustafa Bilal Bayazit,¹ Cécile Jacovetti,¹ Cristina Cosentino,¹ Jonathan Sobel,¹ Kejing Wu,¹ Flora Brozzi,¹ Adriana Rodriguez-Trejo,¹ Lisa Stoll,¹ Claudiane Guay,¹ and Romano Regazzi^{1,2,3,*}

¹Department of Fundamental Neurosciences, University of Lausanne, 1005 Lausanne, Switzerland

²Department of Biomedical Sciences, University of Lausanne, 1005 Lausanne, Switzerland

³Lead contact

*Correspondence: romano.regazzi@unil.ch

<https://doi.org/10.1016/j.celrep.2022.111069>

SUMMARY

tRNA-derived fragments (tRFs) are an emerging class of small non-coding RNAs with distinct cellular functions. Here, we studied the contribution of tRFs to the regulation of postnatal β cell maturation, a critical process that may lead to diabetes susceptibility in adulthood. We identified three tRFs abundant in neonatal rat islets originating from 5' halves (tiRNA-5s) of histidine and glutamate tRNAs. Their inhibition in these islets reduced β cell proliferation and insulin secretion. Mitochondrial respiration was also perturbed, fitting with the mitochondrial enrichment of nuclear-encoded tiRNA-5^{HisGTG} and tiRNA-5^{GluCTC}. Notably, tiRNA-5 inhibition reduced Mpc1, a mitochondrial pyruvate carrier whose knock down largely phenocopied tiRNA-5 inhibition. tiRNA-5^{HisGTG} interactome revealed binding to Musashi-1, which was essential for the mitochondrial enrichment of tiRNA-5^{HisGTG}. Finally, tiRNA-5s were dysregulated in the islets of diabetic and diabetes-prone animals. Altogether, tiRNA-5s represent a class of regulators of β cell maturation, and their deregulation in neonatal islets may lead to diabetes susceptibility in adulthood.

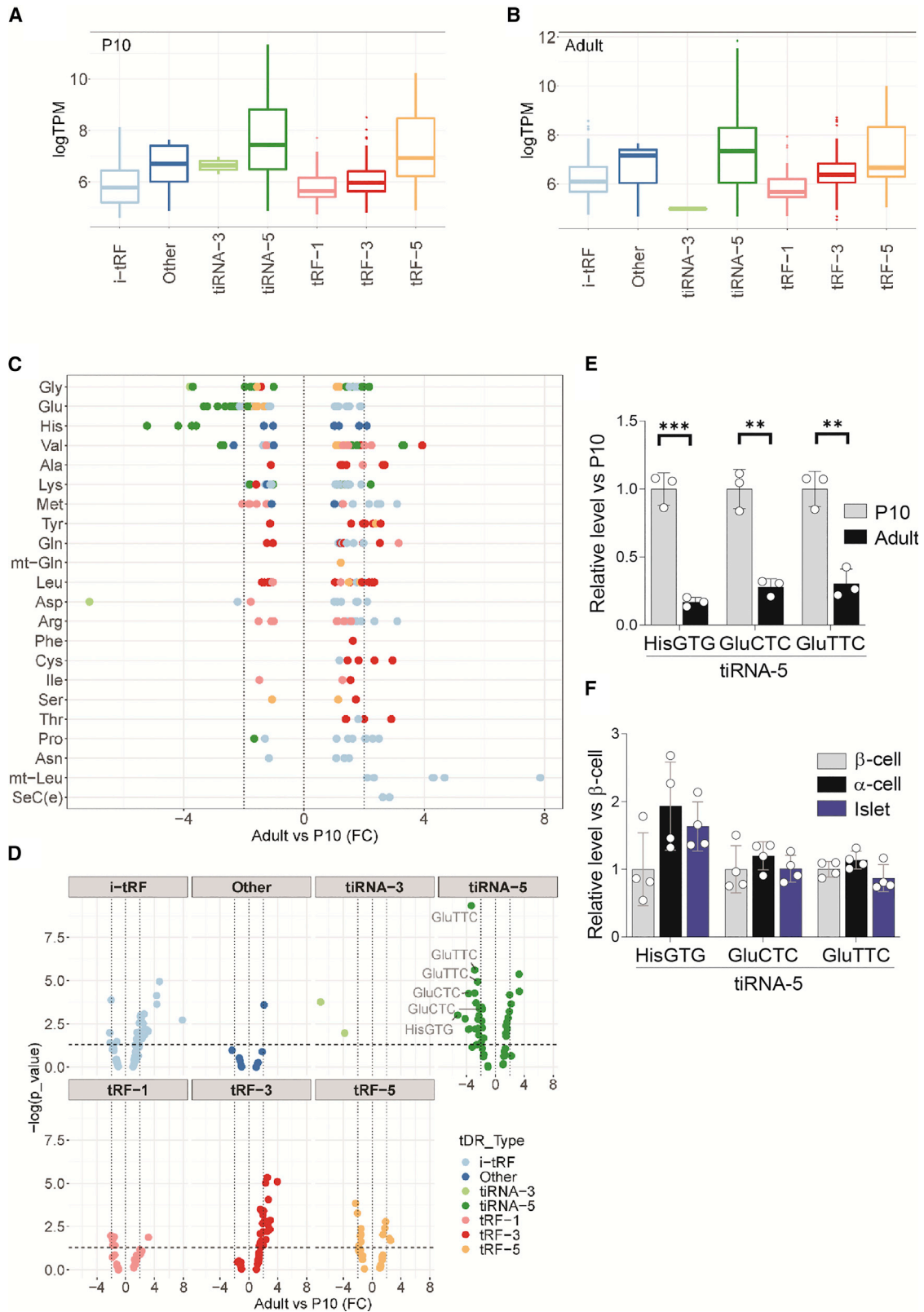
INTRODUCTION

The human genome is composed of 3.2 billion base pairs, of which 76% are transcribed, yet only a tiny proportion (2%) produces proteins (Kapranov et al., 2007). The remaining RNAs constitute the non-coding transcriptome. Initially regarded as futile degradation products of cellular stress, tRNA-derived fragments (tRFs) are now established as a group of conserved short non-coding RNAs regulating various cellular functions (Xie et al., 2020). The most common tRNA fragmentations occur at the loops of mature tRNAs because of programmed cleavage by endonucleases, whose activity may depend on the modification status of the tRNA (Lyons et al., 2018). Angiogenin-mediated cleavage at the anticodon loop yields 29- to 50-nt-long tRNA halves, also known as tiRNAs (Xie et al., 2020). Alternatively, Dicer and other enzymes cleave at the T and D loops to generate 14- to 30-nt-long fragments (Xie et al., 2020). The nomenclature of tRFs is not yet unified. In this manuscript, we will refer to tRNA halves, which are a subset of tRFs, as tiRNA, followed by -3 or -5 , indicating the prime position on the mature tRNA. Functional output of tRFs is cell and condition specific and may occur at epigenetic, translational, and post-translational levels (Kim et al., 2017a; Saikia et al., 2014; Schorn et al., 2017), and regulation of cell proliferation by tiRNA-5s has been described in various models (Honda et al., 2015; Kfoury et al., 2021; Tao et al., 2021). For example, in colorectal cancer cells, hypoxia-

induced tiRNA-5^{HisGTG} targets the expression of tumor suppressor kinase 2 (LATS2) and promotes the activation of oncogenic Hippo signaling pathway (Tao et al., 2021). Alternatively, in osteoblastic cells, genotoxic or infectious stress-induced tiRNA-5^{ProCGG} is packaged within extracellular vesicles and promotes the proliferation of the recipient monocytes by directly interfering with their translational complex (Kfoury et al., 2021).

Pancreatic β cells, which are located in the islets of Langerhans, uniquely produce, store, and secrete insulin in response to elevated blood glucose levels (Marchetti et al., 2017). In the postnatal period, β cells undergo a maturation process that establishes a fully differentiated and functional β cell mass, which can control glucose homeostasis during adulthood (Stolovich-Rain et al., 2015). Neonatal and adult β cells share certain features including insulin content and responsiveness to secretagogues such as L-leucine (Helman et al., 2020; Jacovetti et al., 2015). However, neonatal β cells lack the metabolic profile to efficiently secrete insulin in response to high glucose. In contrast, they possess a strong proliferative capacity that establishes an appropriate β cell mass (Liu and Hebrok, 2017). This transcriptomic rewiring of β cells occurs in parallel with the dietary shift associated with the suckling-weaning transition in rodents (Jacovetti et al., 2015; Stolovich-Rain et al., 2015). Impairments in the proliferative potential of neonatal β cells contribute to diabetes susceptibility in adulthood (William et al., 2012). Accordingly, animal models of maternal malnutrition





(legend on next page)

and intrauterine growth restriction by selective ligation of utero-placental vessels are associated with reduced postnatal β cell proliferation and impaired insulin secretion in adulthood (Boehmer et al., 2017; Theys et al., 2009).

Emerging evidence is pointing to a potential involvement of tRFs in metabolic control. Indeed, a paternal low-protein (LP) diet in mice has been associated with increased tiRNA-5 levels in sperm that repress the endogenous retroelement MERVL during embryogenesis, ultimately contributing to the dysregulation of the offspring's pancreatic islet transcriptome (Sharma et al., 2016). Moreover, methyltransferase TRMT10A deficiency, which is associated with apoptosis of β cells, has been attributed to the increase of tRF-5^{GlnCTG} (Cosentino et al., 2018). Considering the role of tRFs in proliferation and the limited understanding of their role in islet biology, we investigated their potential contribution to neonatal β cell maturation. Our results indicate that a subset of tiRNA-5s are abundant in islets of neonatal rats and are required for efficient neonatal β cell proliferation and insulin secretion. We further illustrate that these nuclear-encoded fragments are enriched in the mitochondrial fractions and modulate the respiratory capacity in neonatal β cells.

RESULTS

tiRNA-5s generated from tRNA^{HisGTG}, tRNA^{GluCTC}, and tRNA^{GluTTC} are downregulated during postnatal β cell maturation

To characterize tRFs potentially implicated in β cell maturation, we analyzed islets of neonatal (postnatal day 10 [P10]) and adult (12 weeks) rats by small RNA sequencing (GEO: GSE163582). The composition of these islets is similar, with a slightly increased proportion of α cells in neonates (Jacovetti et al., 2015). Using this approach, we detected 489 unique tRF reads, 43 of which were differentially abundant upon islet functional maturation (17 downregulated, 26 upregulated). Categorization of these fragments revealed that 5' tRNA halves (tiRNA-5s) were the most abundant class in islets of both P10 and adult rats (Figures 1A and 1B). Cleavage of the anticodon loop can occur at various locations, generating several tiRNA-5s from a single tRNA, a phenomenon previously reported by others (Goodarzi et al., 2015). By analyzing the fragmentation of isoacceptors, we observed that tiRNA-5s are mainly generated by Gly, Glu, His, and Val tRNAs. However, only tiRNA-5^{HisGTG}, tiRNA-5^{GluCTC}, and tiRNA-5^{GluTTC} were collectively skewed toward higher expression in islets of P10 rats (Figure 1C). These accounted for 6 out of the 17 downregulated tRFs in islets of

adult rats (Figure 1D). Due to their high abundance in islets of P10 rats and uniform downregulation in islets of adult rats, these tiRNA-5s were chosen for further analysis, and the changes in their levels were validated by qPCR (Figure 1E). Since islets are composed of different cell types, we sorted islet cells by fluorescence-activated cell sorting (FACS) and observed that tiRNA-5^{GluCTC}, tiRNA-5^{GluTTC}, and tiRNA-5^{HisGTG} levels were comparable in β cells and glucagon-secreting α cells (Figure 1F).

Angiogenin regulates tiRNA-5 levels in islets of P10 rats

Next, mRNA levels of two enzymes important for the cleavage of tRNAs were measured in islets of P10 and adult rats. The ribonuclease Angiogenin cleaves tRNAs at the anticodon to generate tiRNA-5s, a process that may be aided by the demethylase activity of Alkbh3 on anticodon regions (Chen et al., 2019). Like tiRNA-5s, *Angiogenin* was more abundant in islets of P10 rats (Figure 2A), whereas the expression of *Alkbh3* was not changed upon β cell maturation (Figure 2B). Furthermore, knock down of *Angiogenin* in neonatal islets reduced tiRNA-5 levels without affecting those of tRF-3^{AlaAGC}, which belongs to another class of tRFs not predicted to be generated by Angiogenin (Figures 2C and 2D). These results suggest that Angiogenin contributes to the abundance of tiRNA-5s in islets of neonatal rats.

tiRNA-5s are vital for proper β cell proliferation and insulin secretion in islets of P10 rats

To elucidate the biological function of tiRNA-5s, we transfected dispersed islet cells of P10 rats with antisense LNA inhibitors against tiRNA-5^{GluCTC}, tiRNA-5^{HisGTG}, tiRNA-5^{GluTTC} (tiRNA-5 cocktail; Figures S1A–S1D). As illustrated by TUNEL assay, concomitant inhibition of tiRNA-5s did not affect β cell death at basal conditions or in response to pro-inflammatory cytokines (Figure 3A). On the other hand, tiRNA-5 cocktail inhibition significantly reduced the proliferation of β cells from P10 rats, as illustrated by a lower proportion of Ki67⁺ (Figure 3B) and BrdU⁺Ins⁺ cells (Figure S1E). Meanwhile, LNA cocktail inhibition of 3'-derived halves (tiRNA-3^{HisGTG}, tiRNA-3^{GluCTC}, tiRNA-3^{GluTTC}) had no impact on β cell proliferation (Figure S1F). At the protein level, blockade of the tiRNA-5s resulted in a reduction of important regulators of β cell-mass expansion such as phosphorylated Akt and Survivin (Figures 3C and 3D).

Furthermore, the impact of the tiRNA-5s on insulin secretion was investigated. As immature β cells are unable to secrete insulin efficiently in response to glucose alone (Jacovetti et al., 2015), the cells were stimulated with glucose in the presence of a physiological L-leucine concentration (Helman et al., 2020). Inhibition

Figure 1. Identification of tRNA-derived fragments in neonatal and adult islets

(A and B) tRF levels in islets of P10 (A) and adult (B) rats (n = 3). tRFs are classified as tRNA halves (tiRNA), distal (tRF), internal (i-tRF), pre-tRNA (tRF-1), or "other" fragments. TPM, transcripts per million.

(C) Fragmentation profile of isoacceptors. Vertical dashed lines indicate a fold change of ± 2 , with negative values presenting fragments more detected in P10 islets.

(D) Volcano plot of tRFs in islets of P10 and adult rats. Fragments above the horizontal dashed line are significantly changing ($p < 0.05$). Vertical dashed lines indicate a fold change of ± 2 .

(E) Real-time PCR validation of tiRNA-5 downregulation in adult islets. Level in islets of P10 rats was used as a baseline, and miR-7 was used as a housekeeping small non-coding RNA (ncRNA). The data are shown as means \pm SD (n = 4). ** $p < 0.01$, *** $p < 0.001$ by two-tailed unpaired t test.

(F) Levels of tiRNA-5s in FACS α and β cells obtained from rat islets, measured by real-time PCR. β cell level was used as a baseline, and let-7e was used as a housekeeping small ncRNA. Data and mean are represented \pm SD (n = 4).

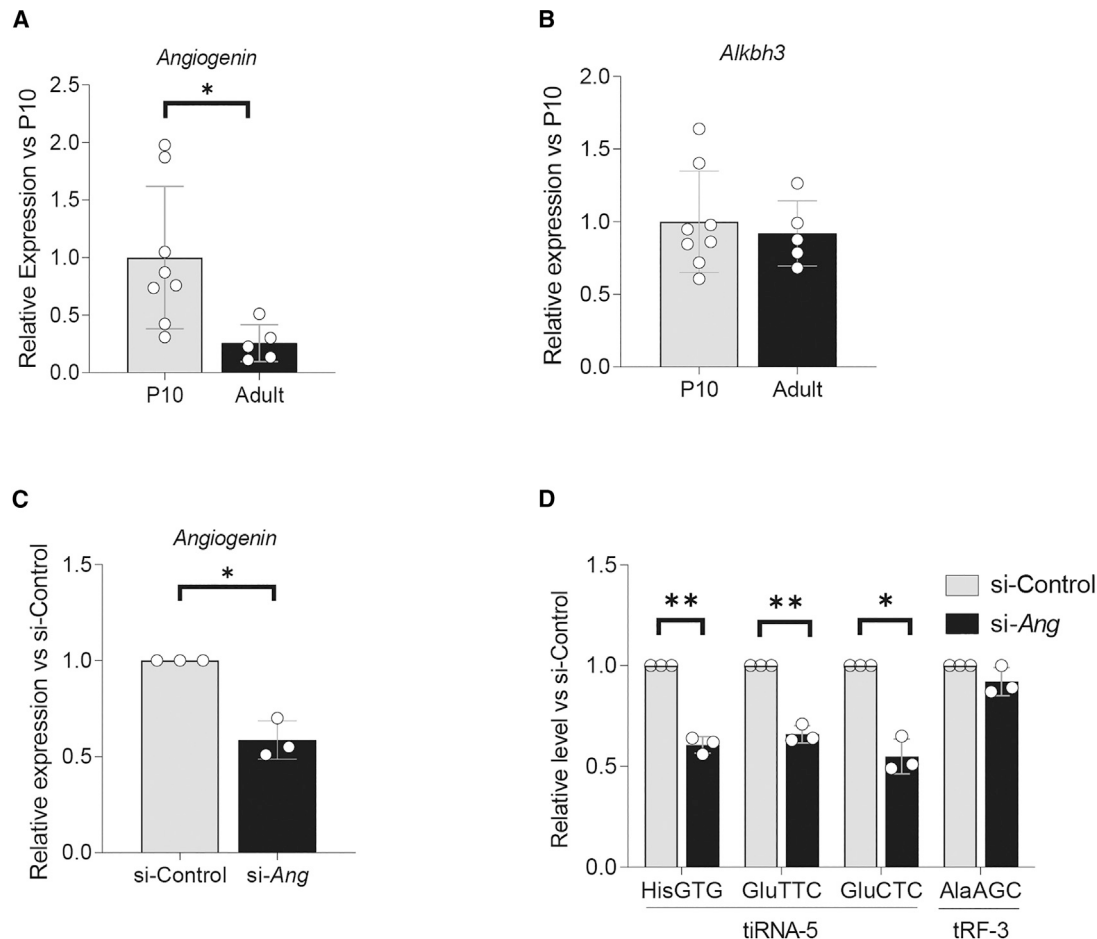


Figure 2. tiRNA-5 levels in rats are correlated to and regulated by Angiogenin

(A and B) Expression of *Angiogenin* (A) and *Alkbh3* (B) in islets of P10 and adult rats measured by qPCR. P10 level used as a baseline, and *Hprt1* used as a housekeeping gene. The data are shown as means \pm SD (n = 5–8).

(C) *Angiogenin* silencing in dispersed islet cells of P10 rats transfected with control (si-Control) or *Angiogenin* (si-Ang) siRNAs for 72 h. *Hprt1* was used as housekeeping gene. The data are shown as means \pm SD (n = 3).

(D) tRF levels in dispersed islet cells of P10 rats transfected with control (si-Control) or *Angiogenin* (si-Ang) siRNAs for 72 h. miR-7 was used as housekeeping small ncRNA. Data and mean are represented \pm SD (n = 3). *p < 0.05, **p < 0.01 by two-tailed unpaired (A and B) and paired (C and D) t tests.

of the tiRNA-5s in islets of P10 rats had no impact on basal insulin secretion, protein content, or insulin content (Figures 3E, S1G, and S1H). However, a decrease in insulin secretion was observed upon stimulatory conditions (Figure 3E). Inhibition of the corresponding 3'-derived halves was without effect, confirming the specificity of tiRNA-5s contribution to neonatal β cell secretion (Figure S1I).

tiRNA-5^{GluCTC} and tiRNA-5^{HisGTG} are enriched in the mitochondria of β cells

To better characterize tiRNA-5s in β cells, we next sought to determine their subcellular localization. Using a protocol that separates nuclear from non-nuclear fractions of INS832/13 cells, a rat β cell line, we determined that tiRNA-5^{GluTTC} is present in both fractions, whereas tiRNA-5^{GluCTC} and tiRNA-5^{HisGTG} are enriched in the non-nuclear fraction (Figure 4A). Moreover, using an approach to distinguish mitochondrial RNA from other

non-nuclear fractions (Figures S2A and S2B), we found that tiRNA-5^{GluCTC} and tiRNA-5^{HisGTG} are highly enriched in the mitochondrial fraction (Figure 4B). In contrast, no enrichment was observed for tiRNA-5^{GluTTC} or miR-106b (Tsukita et al., 2017).

tiRNA-5s are required for efficient mitochondrial respiration in islets of P10 rats

To assess whether tiRNA-5^{GluCTC}, HisGTG, GluTTC inhibition induces mitochondrial dysfunction, mitochondrial respiration was assessed by Seahorse XFp Extracellular Flux Analyzer (Agilent Technologies). Respiration was measured as the oxygen consumption rate (OCR) in a low-glucose (basal) condition, followed by sequential challenges to high glucose/L-leucine and modulators of electron-transport chain oligomycin (ATP synthase inhibitor), carbonyl cyanide-4 (trifluoromethoxy) phenylhydrazone (FCCP) (mitochondrial uncoupler), and rotenone/antimycin A (inhibitors of mitochondrial respiration) (Figure 4C).

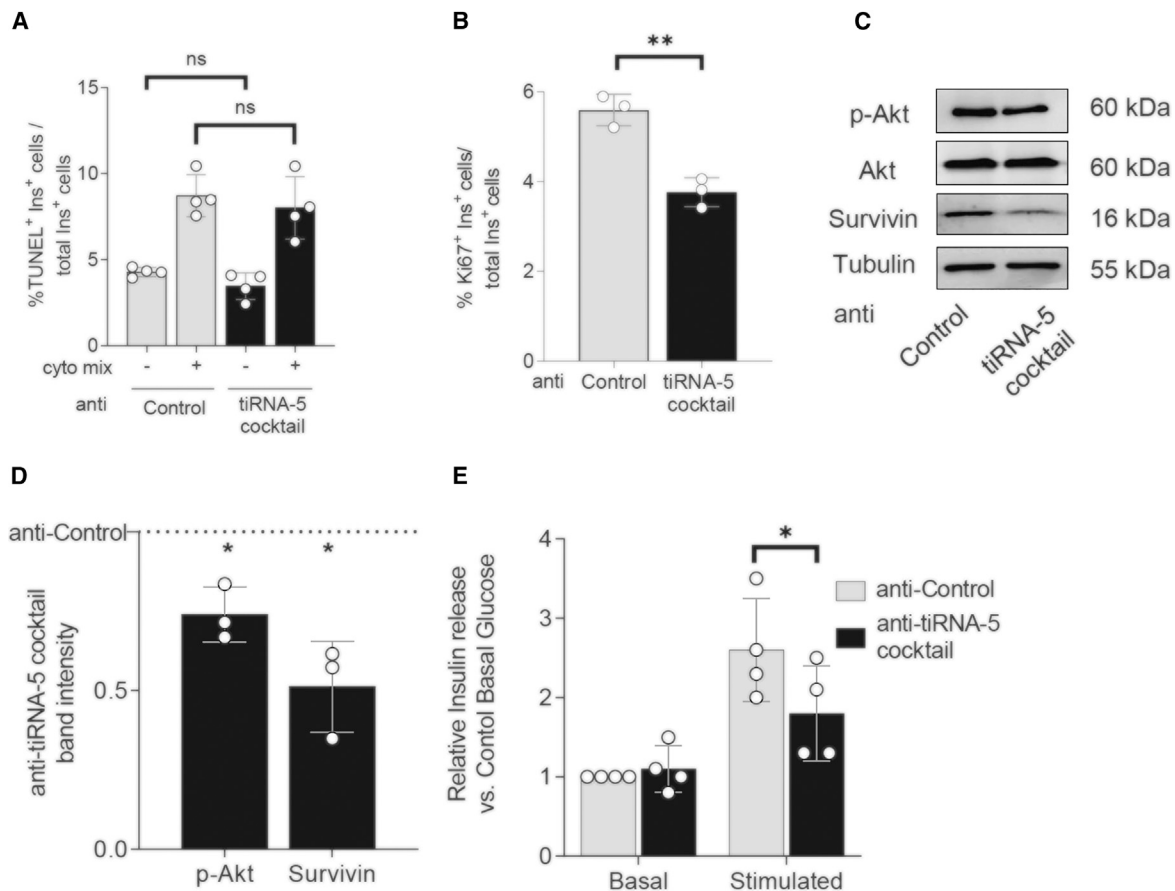


Figure 3. tiRNA-5s are essential for proliferation and insulin secretion of β cells of P10 rats

Dispersed islet cells from P10 rats transfected with anti-control or anti-tiRNA-5 cocktail LNA inhibitors for 72 h.

(A) Basal and 24 h cytokine-induced apoptosis by TUNEL staining. >1,000 insulin⁺ cells counted. The data are shown as means \pm SD (n = 4).

(B) Proliferation assays using Ki-67 immunostaining. >1,000 insulin⁺ cells counted. The data are shown as means \pm SD (n = 3).

(C) Western blot of proliferation markers (representative of three independent repeats).

(D) Quantification of western blots. p-Akt (Ser473) and survivin normalized with Akt and tubulin. The data are shown as means \pm SD (n = 3).

(E) Basal (2 mM glucose) and stimulated (10 mM Glucose and 1 mM L-leucine) insulin secretion. Data are normalized to insulin content. Anti-control basal secretion was used as baseline. Data and mean are represented as \pm SD (n = 4). *p < 0.05, **p < 0.01 by two-tailed paired t test. ns, not significant.

Compared with control cells, tiRNA-5 inhibition induced reductions in basal respiration, ATP production, and maximal respiratory capacity (Figures 4D, 4E, and 4G). The respiratory response to high glucose/L-leucine (Figure 4F), coupling efficiency, and non-mitochondrial oxygen consumption were not significantly altered (Figures S2C and S2D). These results illustrate the role of the tiRNA-5s in mitochondrial respiration.

tiRNA-5 inhibition is associated with a decrease in Mpc1 protein level in islets of P10 rats

To determine the mode of action of the tiRNA-5s, we analyzed the changes in the transcriptomic and proteomic profiles occurring in dispersed islets of P10 rats upon tiRNA-5^{GluTTC, HisGTG, GluTTC} inhibition. No significant changes were observed by mRNA sequencing (cutoff of at least 2-fold, adjusted p < 0.05; Figure 5A; GEO: GSE163584). In contrast, we identified 13 proteins that are differentially expressed (cutoff of at least 2-fold, p < 0.05; Figure 5B; Table S1). Among the top downregulated proteins,

Mpc1, a mitochondrial pyruvate transporter, was reduced by 2.8-fold. These findings were validated by western blotting using an antibody against Mpc1 (Figures 5D and 5E). This effect was specific since transfection of islet cells with oligonucleotides directed against the 3' halves of tRNA^{GluTTC, GluCTC, HisGTG} had no effect on Mpc1 level (Figures S3A and S3B).

The mRNA level of *Mpc1* was not significantly affected by tiRNA-5 inhibition, indicating that tiRNA-5s are likely to regulate Mpc1 expression on a posttranscriptional level (Figure 5F). The levels of neither the Mpc1 co-stabilizing protein Mpc2 nor any other abundant mitochondrial proteins such as Cox4-6 were changed (Table S1), suggesting that the reduction in Mpc1 is highly unlikely to be due to a reduction in mitochondrial mass.

Mpc1 knock down largely phenocopies tiRNA-5 inhibition in islets of P10 rats

To potentially attribute the defective β cell function observed upon tiRNA-5 inhibition to reduced Mpc1 levels, *Mpc1* was

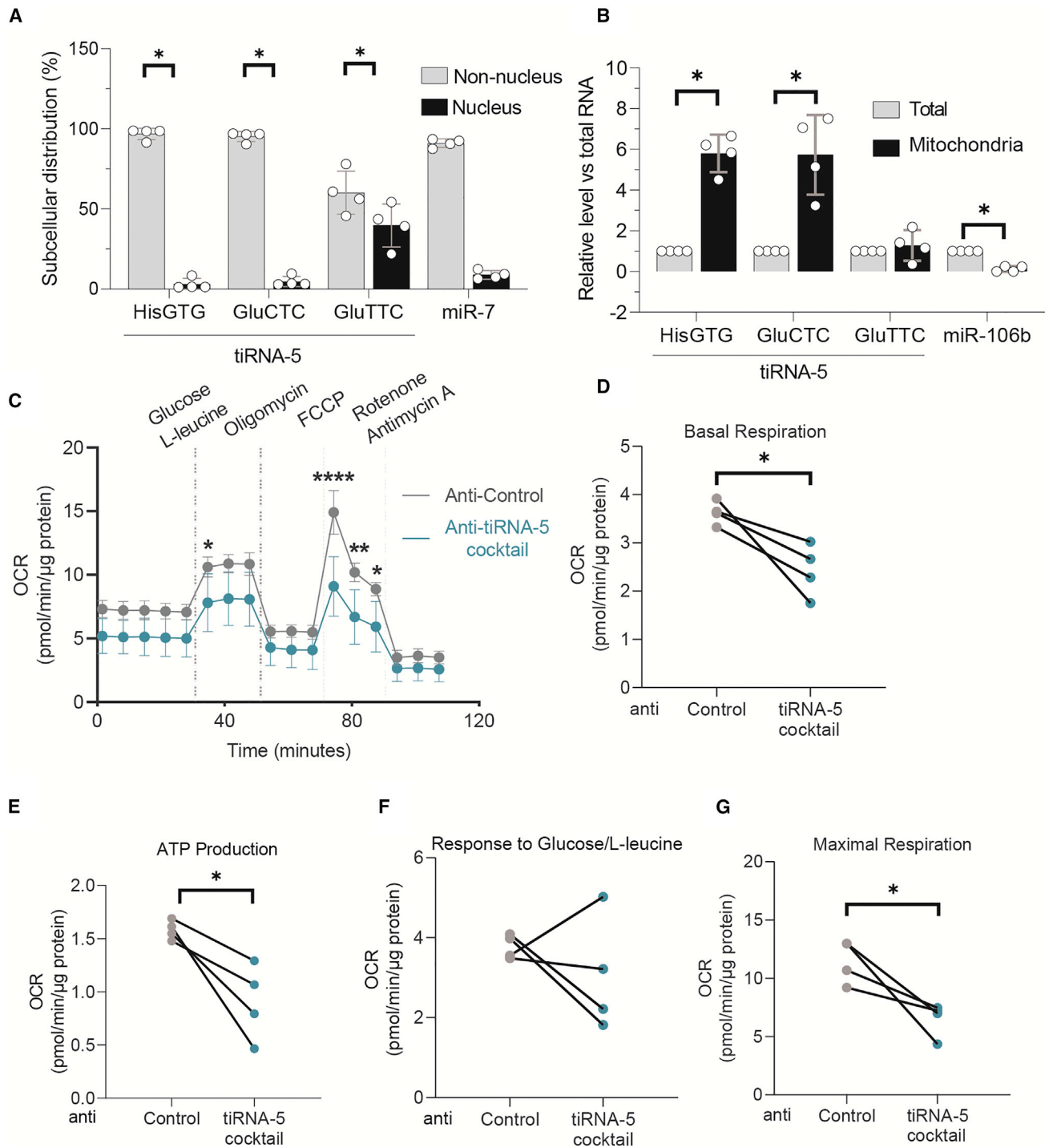


Figure 4. Subcellular localization of tiRNA-5 in β cells, and their impact on mitochondrial respiration in islet cells of P10 rats

(A) tiRNA-5 levels in nuclear fractions of INS832/13 cells. miR-7 is used as a non-nuclear control. The data are shown as means \pm SD (n = 4).

(B) Enrichment of tiRNA-5s in mitochondrial fractions of INS832/13 cells. miR-106b is used as a cytoplasmic control. The data are shown as means \pm SD (n = 4).

(C) OCR profiles of dispersed islet cells of P10 rats (n = 4) transfected with anti-control (gray) or anti-tiRNA-5 cocktail (turquoise) inhibitor for 72 h at basal glucose levels, followed by sequential injections of 20 mM glucose/1 mM L-leucine, 5 μ M oligomycin, 2 μ M FCCP, and 1 μ M rotenone/1 μ M antimycin A at indicated intervals. Data normalized to μ g protein. The data are shown as means \pm SD (n = 4).

(D–G) OCR values used to calculate basal respiration, ATP production, glucose/L-leucine-stimulated, and maximal respiration (n = 4). *p < 0.05, **p < 0.01, ****p < 0.0001 by two-tailed paired t test (A, B, and D–G) or two-way ANOVA (C).

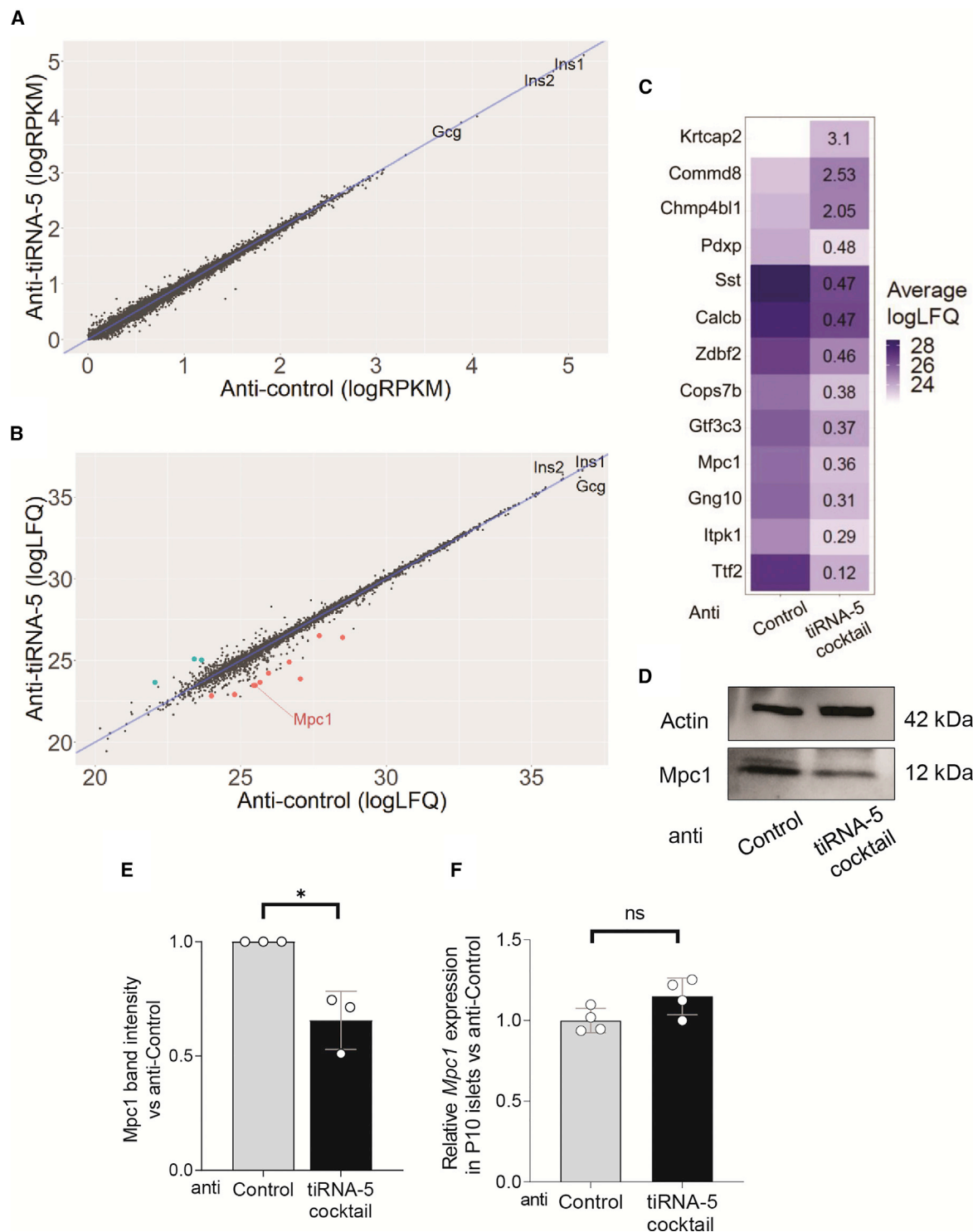


Figure 5. The effect of tiRNA-5 cocktail inhibition on the transcriptome and proteome of islets cells of P10 rats

Dispersed islet cells of P10 rats transfected with anti-control or anti-tiRNA-5 cocktail inhibitors for 72 h (n = 4 per condition).

(A) Scatterplot of RNA-seq analysis. Diagonal line depicts no change.

(B) Scatterplot of mass spectrometry. Diagonal line depicts no change. Significantly changing hits (fold change > 2, p < 0.05) are colored. Green: upregulated; red: downregulated.

(legend continued on next page)

knocked down in dispersed islets of P10 rats using a small interfering RNA (siRNA) (Figure 6A). *Mpc1* knock down also reduced the proliferative capacity of β cells of P10 rats (Figure 6B) and impaired glucose and L-leucine-stimulated insulin secretion without affecting basal secretion (Figure 6C). Furthermore, blockade of mitochondrial pyruvate uptake using MPC inhibitor UK5099 (Vacanti et al., 2014) reduced maximal mitochondrial respiration and ATP production. In contrast, basal respiration rate was not affected (Figures 6D and 6E). To assess whether *Mpc1* interacts with tiRNA-5s, we analyzed the RNAs co-precipitated with *Mpc1*. Upon *Mpc1* immunoprecipitation, an enrichment of tiRNA-5^{HisGTG} was observed (Figures 6F and 6G). Overall, these results indicate that β cell defects observed upon tiRNA-5 inhibition may, in part, be mediated by *Mpc1*.

Interaction of tiRNA-5^{HisGTG} with RNA-binding proteins

As tRFs can regulate biological processes through protein interactions (Jacovetti et al., 2021), we sought to unveil the molecular bases for the tiRNA-5 function by performing RNA pull-down assays in INS832/13 cells coupled to mass spectrometry. A biotinylated oligonucleotide of tiRNA-5^{HisGTG} was used as bait due to its enrichment in mitochondrial fractions and *Mpc1* immunoprecipitation (Figures 7A and 7B). Analysis of the protein interactome revealed 18 RNA-binding proteins (RBPs) significantly enriched (log₂ fold change > 2, adjusted p < 0.05) upon tiRNA-5^{HisGTG} pull-down. These included members of the heterogeneous nuclear ribonucleoprotein (hnRNP) and Musashi (Msi) families, as well as mitochondrial ribosomal proteins (Figures 7C; Table S2). Several of the interacting proteins were verified by western blots (Figure 7D).

Msi1 is essential for the mitochondrial enrichment of tiRNA-5^{HisGTG}

Among tiRNA-5^{HisGTG}-binding proteins, Msi1 and Msi2 are translational regulators of proliferation in various models, including in pancreatic β cells (Kudinov et al., 2017; Szabat et al., 2011). Furthermore, Msi proteins can modulate mitochondrial respiration and microRNA (miRNA) trafficking to mitochondria in different models (Guo et al., 2020; Lang et al., 2017). In line with the literature, silencing *Msi1* in dispersed P10 rat islet cells significantly reduced β cell proliferation (Figures 7E and 7G). While we could not detect a specific enrichment of Msi1 in β cell mitochondria (Figures S4A and S4B), silencing *Msi1* dissipated the accumulation of tiRNA-5^{HisGTG} in the mitochondrial fraction (Figure 7F). This provided a direct molecular basis for the mitochondrial transfer of tiRNA-5^{HisGTG} potentially contributing to the phenotype observed upon tiRNA-5 inhibition in islet cells from P10 rats.

tiRNA-5 levels are altered in pathophysiological models of β cell maturation

Finally, as tiRNA-5s are highly abundant in proliferative neonatal islets, their levels in pathophysiological models of defective β

cell-mass expansion were investigated. Maternal LP diet during gestation and lactation reduces the proliferative capacity of β cells from neonatal rats, thereby preventing the establishment of an appropriate β cell mass (Theys et al., 2009). Feeding rat dams with an LP diet during gestation and lactation drastically reduced the body weight of the pups by P10 (Figure S5A). The levels of tiRNA-5^{GluTTC}, tiRNA-5^{GluCTC}, and tiRNA-5^{HisGTG} were significantly lower in islets of the LP offspring compared with the control-diet group (Figure S5B). Furthermore, an LP diet reduced islet *Alkbh3* expression without significantly changing *Angiogenin* expression (Figure S5C).

While under physiological conditions, the β cell mass is rather constant during adulthood, obesity propels an expansion of the β cells to compensate for the increased metabolic demands. Two established animal models of obesity are normoglycemic leptin-deficient *ob/ob* mice and hyperglycemic leptin-receptor-deficient *db/db* mice (Wang et al., 2014). Compared with healthy *db/+* littermates, tiRNA-5^{GluTTC} level was significantly increased in *db/db* islets, while tiRNA-5^{HisGTG} and tiRNA-5^{GluCTC} were not changed (Figure S5D). On the other hand, no changes in tiRNA-5 levels were observed in the islets of *ob/ob* mice (Figure S5E), suggesting that tiRNA-5s are dispensable for β cell expansion in this model. Altogether, tiRNA-5s levels are altered in the islets of LP rats, which is a relevant pathophysiological model of neonatal β cell-mass expansion.

DISCUSSION

In this study, we investigated whether tRFs contribute to β cell function at a critical time point in β cell development. We identified and focused on three fragments deriving from His and Glu tRNAs based on their high abundance in neonatal islets and downregulation in islets of adult rats. Inhibition of these fragments in dispersed islets of P10 rats reduced β cell proliferation and insulin secretion and perturbed mitochondrial respiration.

To appreciate the role of tiRNA-5s, we modulated their levels in the islets of P10 rats to mimic the profile observed in adults. To do so, we used an LNA-inhibition strategy that does not impact the whole tRNA (Goodarzi et al., 2015), possibly due to the rigid L-shaped tertiary structure of mature tRNAs and their tight binding to elongation factors in the cytoplasm. Indeed, inhibition of 3' halves of the same tRNAs (tiRNA-3s) had no impact on β cell proliferation. We elected not to use an overexpression strategy as endogenous tRF function relies heavily on their modification profile, which may not be replicated with oligonucleotide mimics (Guzzi et al., 2018). We also emphasized on tiRNA-5 function independent of *Angiogenin*. While *Angiogenin* overexpression is sufficient to recover cytokine-mediated proliferative defects in β cells (Rutti et al., 2018), it has other essential functions within cells, including ribosomal RNA transcription (Kishimoto et al., 2005). Hence, it would be infeasible to specifically delineate tiRNA-5 function in *Angiogenin* models.

(C) List of significantly changing proteins (at least 2-fold change, p < 0.05).

(D) Confirmation of *Mpc1* downregulation by western blot (representative of three independent experiments).

(E) Quantification of western blots. *Mpc1* levels are normalized to actin. The results are shown as means \pm SD (n = 3).

(F) *Mpc1* level measured by qPCR. Control islets used as baseline. *Hprt1* used as a housekeeping gene. Data and mean are represented \pm SD (n = 4). *p < 0.05 by two-tailed paired t test. ns, not significant.

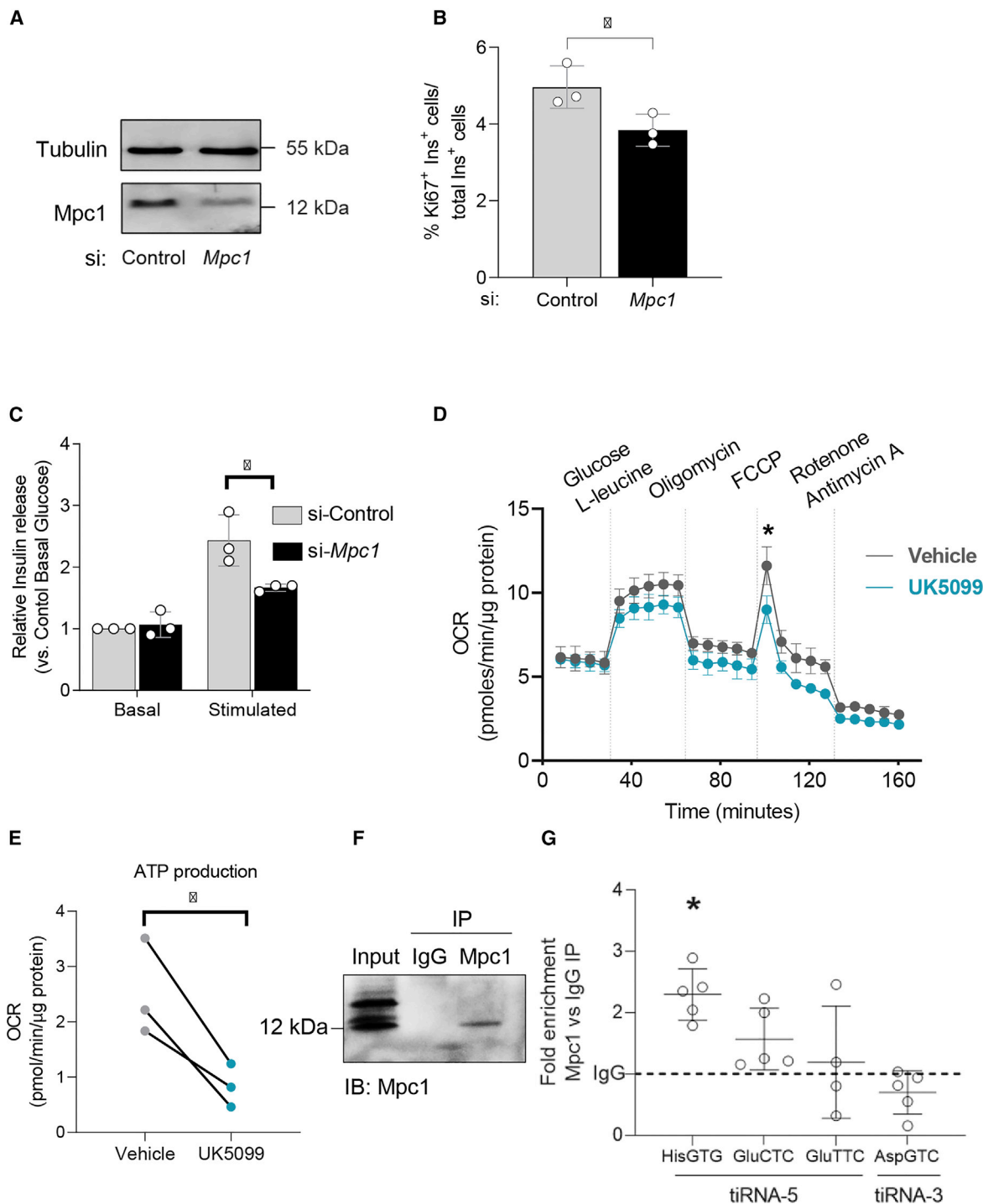


Figure 6. Impact of *Mpc1* knock down in dispersed islet cells of P10 rats

(A–C) Dispersed islet cells from P10 rats were transfected with si-control or si-*Mpc1* for 72 h.

(A) *Mpc1* knockdown confirmation by western blot.

(B) Proliferation of β cells as determined by Ki-67 staining. At least 1,000 insulin-positive cells were counted. The results are presented as means \pm SD (n = 3).

(C) Basal (2 mM Glucose) and stimulated (10 mM glucose and 1 mM L-leucine) insulin secretion. Data normalized to insulin content. Si-control basal secretion used as baseline. The results are the means \pm SD (n = 3).

(D) OCR profiles of dispersed islet cells from P10 rats treated with vehicle (gray) or 150 μ M UK5099 (turquoise) at basal glucose levels, followed by sequential injections of 20 mM glucose/1 mM L-leucine, 5 μ M oligomycin, 2 μ M FCCP, and 1 μ M rotenone/1 μ M antimycin A at indicated intervals (dashed lines). Data normalized to μ g protein. The results are presented as means \pm SD (n = 3).

(legend continued on next page)

Importantly, tiRNA-5 inhibition decreased the proliferative capacity of β cells of P10 rats, suggesting that the critical β cell-mass expansion occurring in the neonatal period may be impaired if tiRNA-5 levels cannot be maintained. The effect of tiRNA-5s is generally attributed to translational repression as a rapid reaction to cellular stress (Ivanov et al., 2011). However, dichotomous roles of tiRNA-5s in cell proliferation have been reported. For example, upregulation of tiRNA-5^{GlyGCC} reduces the proliferation of hematopoietic stem cells by inducing a global suppression of protein synthesis (Goncalves et al., 2016). In contrast, the same tiRNA-5 promotes proliferation of breast cancer cells (Honda et al., 2015). Furthermore, tiRNA-5^{HisGTG} is reported to promote hippo signaling proliferation in colorectal cancer cells and xenografts through targeting large tumor suppressor kinase 2 (LATS2) (Tao et al., 2021). Therefore, tiRNA-5s need to be studied in a cell-specific manner, where the microenvironment may propel tiRNA-5s to exert unique effects.

The functions of tRFs generated from the nuclear-encoded tRNAs have only been studied in the nucleus or the cytoplasm. However, other non-coding RNAs such as tRNAs and miRNAs are actively transported to the mitochondria (Kim et al., 2017b). This prompted us to measure tiRNA-5 levels in mitochondrial fractions of β cells, where we indeed observed an enrichment of tiRNA-5^{HisGTG} and tiRNA-5^{GluCTC}. To our knowledge, this is the first suggestion of the transfer of a nuclear-encoded tRF to mitochondria.

It has previously been reported that immature β cells have a higher level of mitochondrial oxygen consumption and ATP production than mature β cells at basal levels of glucose (Stolovich-Rain et al., 2015). Importantly, in the absence of the tiRNA-5s in islets of P10 rats, we have observed a divergence from this key characteristic of immature β cells, as both basal mitochondrial oxygen consumption and ATP production were reduced. Furthermore, the maximal respiration was significantly reduced, suggesting that the cell may not be able to achieve rapid oxidation of substrates upon a metabolic challenge. Altogether, the perturbed respiratory capacity and ATP production may contribute to the observed defects in β cell proliferation and insulin secretion. It is important to note that after a 72 h tiRNA-5 inhibition, the β cell-proliferation rate drops from 5.7% to 3.8% in the islets of neonatal rats. This change is not yet sufficient to reflect on the total islet protein content or on the content of β cell identity proteins, such as insulin (Table S1), suggesting that the respiratory defect is not due to a reduction in β cell mass.

To better characterize the molecular signatures of the observed phenotypes, we have performed proteomic and transcriptomic analyses. Mpc1, a vital pyruvate carrier located in the inner mitochondrial membrane, was among the 13 differentially expressed proteins. Mpc1 and its co-stabilizing protein Mpc2 form a hetero-oligomeric complex that assembles on the inner mitochondrial membrane (Bricker et al., 2012). This com-

plex links glycolysis to oxidative phosphorylation (OXPHOS) by importing pyruvate into the mitochondrial matrix to be incorporated into the tricarboxylic acid (TCA) cycle. Previously, a defect in glucose-stimulated insulin secretion was observed in the islets of *Mpc2* hypomorphic mice (Vigueira et al., 2014), as well as in human and rat islet cells treated with an siRNA against *Mpc1* or with pharmacological inhibitors of the MPC complex (Brun et al., 2015). Notably, the islets of β cell-specific *Mpc2* knockout mice are associated with a decreased glucose-induced respiration, an ATP-sensitive potassium channel hyperactivity, and an impaired insulin secretion (McCommis et al., 2016). The MPC complex has been shown to function as a Warburg-suppressive unit in highly glycolytic cancer cells (Bensard et al., 2020). In contrast to cancer cells, β cells are more lipogenic, less glycolytic, and more reliant on OXPHOS (Rutter et al., 2015). Accordingly, *Mpc1* inhibition attenuates mTORC1 signaling in the INS-1E β cell line (Rumala et al., 2020), suggesting that MPC may fuel, rather than suppress, cell growth in β cells. In agreement with this hypothesis, targeting *Mpc1* in islets of P10 rats largely phenocopied the inhibition of the tiRNA-5s and reduced β cell proliferation. This suggests that the phenotypes observed upon tiRNA-5 inhibition may, in part, stem from incomplete pyruvate import into the mitochondria.

The emergence of proteomic analyses on tRF-immunoprecipitated samples has led to the identification of new potential targets of tRFs (Chen et al., 2019; Krishna et al., 2019). Using a similar approach, we identified the interacting proteins of tiRNA-5^{HisGTG}, which was highly enriched in the mitochondrial fraction. It is noteworthy that *Mpc1* was not detected in our tiRNA-5 pull-down assay, possibly due to a higher affinity of tiRNA-5s to RBPs within this setting. Identification of proteins acting on various pathways may be indicative of a synergistic effect contributing to the tiRNA-5-mediated phenotype. Among these, *Msi1* and *Msi2* are critical proliferation regulators. We specifically focused on *Msi1*, as we could confirm its interaction to tiRNA-5^{HisGTG} by western blot. The function of the *Msi1* has mostly been attributed to modulation of Notch signaling pathway (Kudinov et al., 2017). Particularly, in the MIN6 mouse β cell line, *Msi1* stimulates proliferation through upregulation of *Hes1*, a key regulator of the Notch signaling pathway (Szabat et al., 2011). *Msi1* silencing indeed attenuated neonatal β -cell proliferation. However, no significant changes in the components of Notch signaling pathway were observed upon tiRNA-5 inhibition, as shown by proteomic profile. This suggests other ways in which the *Msi1*-tiRNA-5^{HisGTG} interaction is functionally relevant. Interestingly, we found that *Msi1* is essential for the mitochondrial enrichment of tiRNA-5^{HisGTG}. This finding is in line with a recent report on *MSI2* transporting miR-301a-3p to mitochondria in human umbilical vein endothelial cells (HUVECs) (Guo et al., 2020).

Considering the essential role of mitochondrial metabolism in differentiation and development, how tiRNA-5s impact mitochondrial function remains an important and outstanding

(E) OCR values in (D) used to calculate ATP production.

(F) Immunoblotting (IB) of *Mpc1* upon *Mpc1* or control immunoglobulin G (IgG) immunoprecipitation (IP) in INS832/13 cells. 10% cell lysate loaded as input.

(G) qPCR of tRFs upon *Mpc1* or IgG IP. IgG IP used as a baseline. Data and mean are represented \pm SD (n = 5). *p < 0.05 by two-tailed paired t test (B, C, E, and F) or two-way ANOVA (D).

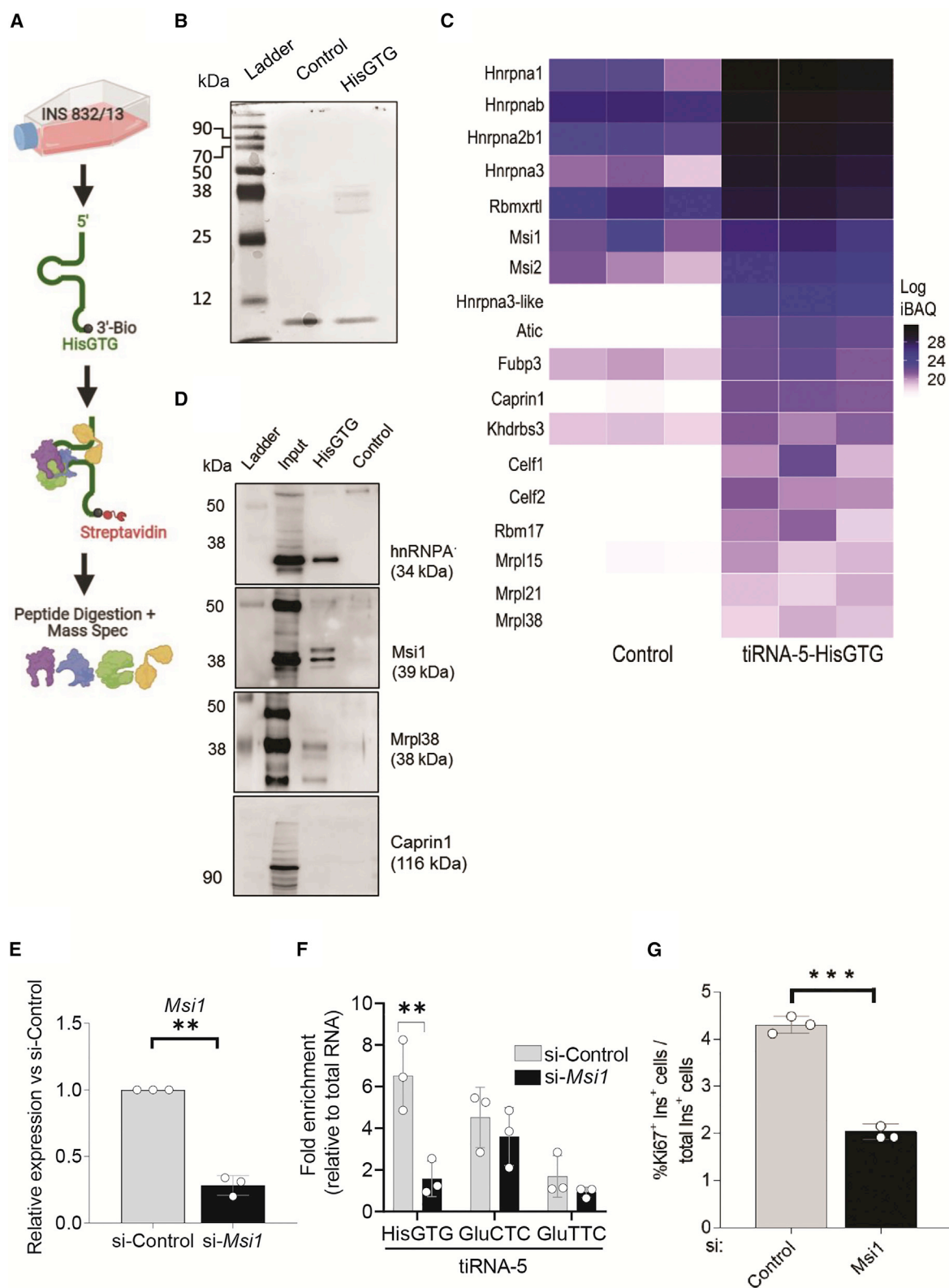


Figure 7. Identification of tiRNA-5^{HisGTG}-interacting proteins

(A) Workflow of *in vitro* pull down. INS832/13 cell lysates incubated with 3' biotinylated tiRNA-5^{HisGTG} oligonucleotide or its scrambled control. Proteins pulled down with streptavidin beads and either visualized on an SDS-PAGE or analyzed by mass spectrometry.

(legend continued on next page)

question. Within the cytosol, tiRNA-5s interfere with the stability of the translational complexes through their interactions with various factors and ribosomal proteins (Chen et al., 2019). A similar mechanism may also be relevant for mitochondrial translation. In fact, a set of mitochondrial ribosomal proteins were among the identified targets of tiRNA-5^{HisGTG}. Mitochondrial DNA encodes for 13 proteins essential for OXPHOS. Future studies analyzing their translation efficiency and stability in the absence of tiRNA-5s are necessary to delineate the potential role of tiRNA-5s in mitochondrial translation.

Finally, we have illustrated that tiRNA-5 levels are dysregulated in the islets of *db/db* mice and in the offspring of rat dams kept on an LP diet. The upregulation of tiRNA-5^{GluTTC}, as well as the upregulation tendency of other tiRNA-5s, in *db/db* islets and not normoglycemic *ob/ob* islets may be due to the dedifferentiated state of β cells from *db/db* islets (Talchai et al., 2012), which resemble β cells from P10 rats. These results suggest that tiRNA-5s are implicated in pathophysiological models of β cell-mass expansion.

In conclusion, a global profiling of tRFs in islets of neonatal and adult rat islets allowed us to identify tiRNA-5s as key regulators of neonatal β cell proliferation, a critical event to achieve a sufficient β cell mass to avoid blood glucose homeostasis deficiencies leading to diabetes. Furthermore, we highlight mitochondrial enrichment of certain tiRNA-5s and regulation of mitochondrial function. This may pave the way for identifying new regulations of mitochondrial pyruvate metabolism driving metabolic reprogramming in various cell types.

Limitations of the study

Here, we highlight the impact of tiRNA-5s on β cell function in an *ex vivo* setting. We further illustrate that tiRNA-5 levels are implicated in relevant pathophysiological conditions. Whether these tiRNA-5s regulate functional β cell mass *in vivo* is yet to be proven.

It is noteworthy that a set of splicing factors belonging to the hnRNP family were identified in the tiRNA-5^{HisGTG} interactome. These are highly abundant and predominantly nuclear proteins that attach to various RNAs in pull-down-based approaches (Guzzi et al., 2018; Geuens et al., 2016). However, we cannot rule out any changes in the alternative splicing landscape contributing to the phenotypes observed in neonatal islets. While we did not study these splicing factors any further, certain hnRNPs are detected within the mitochondria (Klimek-Tomczak, et al., 2006; Xavier and Martinou, 2021). Whether tiRNA-5s are implicated in potential mitochondrial effects of hnRNPs is unknown.

Another outstanding question that remains unanswered is through which mechanism tiRNA-5s regulate Mpc1 levels. Further studies replenishing Mpc1 levels upon tiRNA-5 knock down may help establish this relationship.

STAR★METHODS

Detailed methods are provided in the online version of this paper and include the following:

- KEY RESOURCES TABLE
- RESOURCE AVAILABILITY
 - Lead contact
 - Materials availability
 - Data and code availability
- EXPERIMENTAL MODEL AND SUBJECT DETAILS
 - Ethical statement
 - Rats
- METHOD DETAILS
 - Pancreatic islet isolation and culture
 - Cell culture
 - Small RNA-sequencing
 - tRF quantification
 - Inhibition of tRFs
 - siRNA treatment
 - Immunocytochemistry
 - Insulin secretion and insulin ELISA
 - RNA sequencing
 - Protein digestion for mass spectrometry
 - Liquid Chromatography-tandem mass spectrometry (LC-MS)
 - MS analysis
 - Western blotting
 - Mitochondrial fractionation
 - Mitochondrial respiration
 - Identification of tiRNA-5^{HisGTG} interacting proteins
 - tiRNA-5^{HisGTG} pull-down and Mass Spectrometry
- QUANTIFICATION AND STATISTICAL ANALYSIS

SUPPLEMENTAL INFORMATION

Supplemental information can be found online at <https://doi.org/10.1016/j.celrep.2022.111069>.

ACKNOWLEDGMENTS

We thank Dr. D. Ross Laybutt (Garvan Institute of Medical Research, Sydney, Australia) for providing islet RNA samples from *db/db*, *ob/ob*, and

(B) Representative scan of ponceau S staining upon tiRNA-5^{HisGTG} (HisGTG) or scrambled tiRNA-5^{HisGTG} (control) pull down. Proteins run on an SDS-PAGE.
 (C) tiRNA-5^{HisGTG} (HisGTG) or scrambled tiRNA-5^{HisGTG} (control) interactome identified by mass spectrometry. Only proteins significantly enriched upon tiRNA-5^{HisGTG} pull down are visualized (\log_2 fold change > 2, adjusted $p < 0.05$).
 (D) Verification of tiRNA-5^{HisGTG}-interacting proteins by western blot.
 (E) Western blot confirmation of *Msi1* knockdown in dispersed islet cells of P10 rats transfected with si-control or si-*Msi1* for 72 h. The results are presented as means \pm SD ($n = 3$).
 (F) Impact of *Msi1* knock down on the mitochondrial enrichment of tiRNA-5s in INS832/13 cells transfected with si-control or si-*Msi1*. The results are presented as means \pm SD ($n = 3$).
 (G) Proliferation of β cells as determined by Ki-67 staining in dispersed islet cells of P10 rats transfected with si-control or si-*Msi1* for 72 h. > 1,000 insulin⁺ cells counted. The results are means \pm SD ($n = 3$). ** $p < 0.01$, *** $p < 0.001$ by two-tailed paired t test.

age-matched control mice. This work was supported by the Swiss National Science Foundation (310030_188447 to R.R.) and by the Société Francophone du Diabète and Antadir (to C.G.).

AUTHOR CONTRIBUTIONS

R.R. and M.B.B. designed the experiments. M.B.B., C.J., C.C., J.S., F.B., A.R.-T., L.S., K.W., and C.G. performed the experiments and/or analyzed the data. R.R. and M.B.B. wrote the manuscript.

DECLARATION OF INTERESTS

The authors declare no conflict of interest.

Received: January 27, 2021

Revised: February 3, 2022

Accepted: June 17, 2022

Published: July 12, 2022

REFERENCES

- Bensard, C.L., Wisidagama, D.R., Olson, K.A., Berg, J.A., Krah, N.M., Schell, J.C., Nowinski, S.M., Fogarty, S., Bott, A.J., Wei, P., et al. (2020). Regulation of tumor initiation by the mitochondrial pyruvate carrier. *Cell Metabol.* *31*, 284–300.e7, e287. <https://doi.org/10.1016/j.cmet.2019.11.002>.
- Boehmer, B.H., Limesand, S.W., and Rozance, P.J. (2017). The impact of IUGR on pancreatic islet development and beta-cell function. *J. Endocrinol.* *235*, R63–R76. <https://doi.org/10.1530/JOE-17-0076>.
- Bricker, D.K., Taylor, E.B., Schell, J.C., Orsak, T., Boutron, A., Chen, Y.-C., Cox, J.E., Cardon, C.M., Van Vranken, J.G., Dephore, N., et al. (2012). A mitochondrial pyruvate carrier required for pyruvate uptake in yeast, *Drosophila*, and humans. *Science* *337*, 96–100. <https://doi.org/10.1126/science.1218099>.
- Brun, T., Li, N., Jourdain, A.A., Gaudet, P., Duhamel, D., Meyer, J., Bosco, D., and Maechler, P. (2015). Diabetogenic milieu induce specific changes in mitochondrial transcriptome and differentiation of human pancreatic islets. *Hum. Mol. Genet.* *24*, 5270–5284. <https://doi.org/10.1093/hmg/ddv247>.
- Chen, Z., Qi, M., Shen, B., Luo, G., Wu, Y., Li, J., Lu, Z., Zheng, Z., Dai, Q., and Wang, H. (2019). Transfer RNA demethylase ALKBH3 promotes cancer progression via induction of tRNA-derived small RNAs. *Nucleic Acids Res.* *47*, 2533–2545. <https://doi.org/10.1093/nar/gky1250>.
- Cosentino, C., Toivonen, S., Diaz Villamil, E., Ravanat, J.-L., Demine, S., Pachera, N., Schiavo, A., Deglasse, J.-P., Jonas, J.-C., Deglasse, J.P., et al. (2018). Pancreatic β -cell tRNA hypomethylation and fragmentation link TRMT10A deficiency with diabetes. *Nucleic Acids Res.* *46*, 10302–10318. <https://doi.org/10.1093/nar/gky839>.
- Geuens, T., Bouhy, D., and Timmerman, V. (2016). The hnRNP family: insights into their role in health and disease. *Hum. Genet.* *135*, 851–867.
- Goncalves, K.A., Silberstein, L., Li, S., Severe, N., Hu, M.G., Yang, H., Scadden, D.T., and Hu, G.-F. (2016). Angiogenin promotes hematopoietic regeneration by dichotomously regulating quiescence of stem and progenitor cells. *Cell* *166*, 894–906. <https://doi.org/10.1016/j.cell.2016.06.042>.
- Goodarzi, H., Liu, X., Nguyen, H., Fish, L., and Tavazoie, S. (2015). Endogenous tRNA-derived fragments suppress breast cancer progression via YBX1 displacement. *Cell* *161*, 790–802. <https://doi.org/10.1016/j.cell.2015.02.053>.
- Goodyer, W., Gu, X., Liu, Y., Bottino, R., Crabtree, G., and Kim, S. (2012). Neonatal β cell development in mice and humans is regulated by calcineurin/NFAT. *Dev. Cell* *23*, 21–34. <https://doi.org/10.1016/j.devcel.2012.05.014>.
- Gotoh, M., Maki, T., Satomi, S., Porter, J., Bonner-Weir, S., O'Hara, C.J., and Monaco, A.P. (1987). Reproducible high yield of rat islets by stationary in vitro digestion following pancreatic ductal or portal venous collagenase injection. *Transplantation* *43*, 725–730. <https://doi.org/10.1097/00007890-198705000-00024>.
- Guay, C., Kruit, J.K., Rome, S., Menoud, V., Mulder, N.L., Jurdzinski, A., Mancarella, F., Sebastiani, G., Donda, A., Gonzalez, B.J., et al. (2019). Lymphocyte-derived exosomal MicroRNAs promote pancreatic beta cell death and may contribute to type 1 diabetes development. *Cell Metab.* *29*, 348–361.e6. <https://doi.org/10.1016/j.cmet.2018.09.011>.
- Guo, Q.Q., Gao, J., Wang, X.W., Yin, X.L., Zhang, S.C., Li, X., Chi, L.L., Zhou, X.M., Wang, Z., and Zhang, Q.Y. (2020). RNA-binding protein MSI2 binds to miR-301a-3p and facilitates its distribution in mitochondria of endothelial cells. *Front. Mol. Biosci.* *7*, 609828. <https://doi.org/10.3389/fmolb.2020.609828>.
- Guzzi, N., Cieřla, M., Ngoc, P.C.T., Lang, S., Arora, S., Dimitriou, M., Pimková, K., Sommarin, M.N.E., Munita, R., Lubas, M., et al. (2018). Pseudouridylation of tRNA-derived fragments steers translational control in stem cells. *Cell* *173*, 1204–1216.e26. <https://doi.org/10.1016/j.cell.2018.03.008>.
- Helman, A., Cangelosi, A.L., Davis, J.C., Pham, Q., Rothman, A., Faust, A.L., Straubhaar, J.R., Sabatini, D.M., and Melton, D.A. (2020). A nutrient-sensing transition at birth triggers glucose-responsive insulin secretion. *Cell Metabol.* *31*, 1004–1016.e5. <https://doi.org/10.1016/j.cmet.2020.04.004>.
- Hohmeier, H.E., Mulder, H., Chen, G., Henkel-Rieger, R., Prentki, M., and Newgard, C.B. (2000). Isolation of INS-1-derived cell lines with robust ATP-sensitive K⁺ channel-dependent and -independent glucose-stimulated insulin secretion. *Diabetes* *49*, 424–430. <https://doi.org/10.2337/diabetes.49.3.424>.
- Honda, S., Loher, P., Shigematsu, M., Palazzo, J.P., Suzuki, R., Imoto, I., Rigoutsos, I., and Kirino, Y. (2015). Sex hormone-dependent tRNA halves enhance cell proliferation in breast and prostate cancers. *Proc. Natl. Acad. Sci. USA* *112*, E3816–E3825. <https://doi.org/10.1073/pnas.1510077112>.
- Ivanov, P., Emara, M., Villen, J., Gygi, S., and Anderson, P. (2011). Angiogenin-induced tRNA fragments inhibit translation initiation. *Mol. Cell* *43*, 613–623. <https://doi.org/10.1016/j.molcel.2011.06.022>.
- Jacovetti, C., Bayazit, M.B., and Regazzi, R. (2021). Emerging classes of small non-coding RNAs with potential implications in diabetes and associated metabolic disorders. *Front. Endocrinol.* *12*, 670719. <https://doi.org/10.3389/fendo.2021.670719>.
- Jacovetti, C., Matkovich, S.J., Rodriguez-Trejo, A., Guay, C., and Regazzi, R. (2015). Postnatal beta-cell maturation is associated with islet-specific microRNA changes induced by nutrient shifts at weaning. *Nat. Commun.* *6*, 8084. <https://doi.org/10.1038/ncomms9084>.
- Kapranov, P., Willingham, A.T., and Gingeras, T.R. (2007). Genome-wide transcription and the implications for genomic organization. *Nat. Rev. Genet.* *8*, 413–423. <https://doi.org/10.1038/nrg2083>.
- Kfoury, Y.S., Ji, F., Mazzola, M., Sykes, D.B., Scherer, A.K., Anselmo, A., Akiyama, Y., Mercier, F., Severe, N., Kokkalis, K.D., et al. (2021). tRNA signaling via stress-regulated vesicle transfer in the hematopoietic niche. *Cell Stem Cell* *28*, 2090–2103.e9. <https://doi.org/10.1016/j.stem.2021.08.014>.
- Kim, H.K., Fuchs, G., Wang, S., Wei, W., Zhang, Y., Park, H., Roy-Chaudhuri, B., Li, P., Xu, J., Chu, K., et al. (2017a). A transfer-RNA-derived small RNA regulates ribosome biogenesis. *Nature* *552*, 57–62. <https://doi.org/10.1038/nature25005>.
- Kim, K.M., Noh, J.H., Abdelmohsen, K., and Gorospe, M. (2017b). Mitochondrial noncoding RNA transport. *BMB Rep.* *50*, 164–174. <https://doi.org/10.5483/bmbrep.2017.50.4.013>.
- Kishimoto, K., Liu, S., Tsuji, T., Olson, K.A., and Hu, G.-F. (2005). Endogenous angiogenin in endothelial cells is a general requirement for cell proliferation and angiogenesis. *Oncogene* *24*, 445–456. <https://doi.org/10.1038/sj.onc.1208223>.
- Klimek-Tomczak, K., Mikula, M., Dzwonek, A., Paziewska, A., Wyrwicz, L.S., Hennig, E.E., and Ostrowski, J. (2006). Mitochondria-associated satellite I RNA binds to hnRNP K protein. *Acta Biochim. Pol.* *53*, 169–178.
- Krishna, S., Yim, D.G., Lakshmanan, V., Tirumalai, V., Koh, J.L., Park, J.E., Cheong, J.K., Low, J.L., Lim, M.J., Sze, S.K., et al. (2019). Dynamic expression of tRNA-derived small RNAs define cellular states. *EMBO Rep.* *20*, e47789. <https://doi.org/10.15252/embr.201947789>.
- Kudinov, A.E., Karanicolas, J., Golemis, E.A., and Bumber, Y. (2017). Musashi RNA-binding proteins as cancer drivers and novel therapeutic targets. *Clin.*

- Cancer Res. 23, 2143–2153. <https://doi.org/10.1158/1078-0432.CCR-16-2728>.
- Kulak, N.A., Pichler, G., Paron, I., Nagaraj, N., and Mann, M. (2014). Minimal, encapsulated proteomic-sample processing applied to copy-number estimation in eukaryotic cells. *Nat. Methods* 11, 319–324. <https://doi.org/10.1038/nmeth.2834>.
- Lampf, T., Crum, J.A., Davis, T.A., Milligan, C., and Del Gaizo Moore, V. (2015). Isolation and functional analysis of mitochondria from cultured cells and mouse tissue. *J. of Vis. Exp.* 97, e52076. <https://doi.org/10.3791/52076>.
- Lang, Y., Kong, X., He, C., Wang, F., Liu, B., Zhang, S., Ning, J., Zhu, K., and Xu, S. (2017). Musashi1 promotes non-small cell lung carcinoma malignancy and chemoresistance via activating the Akt signaling pathway. *Cell. Physiol. Biochem.* 44, 455–466. <https://doi.org/10.1159/000485012>.
- Liu, J.S.E., and Hebrok, M. (2017). All mixed up: defining roles for β -cell subtypes in mature islets. *Genes Develop.* 31, 228–240. <https://doi.org/10.1101/gad.294389.116>.
- Lyons, S.M., Fay, M.M., and Ivanov, P. (2018). The role of RNA modifications in the regulation of tRNA cleavage. *FEBS Lett.* 592, 2828–2844. <https://doi.org/10.1002/1873-3468.13205>.
- Marchetti, P., Bugliani, M., De Tata, V., Suleiman, M., and Marselli, L. (2017). Pancreatic beta cell identity in humans and the role of type 2 diabetes. *Front. Cell Dev. Biol.* 5, 55. <https://doi.org/10.3389/fcell.2017.00055>.
- McCommis, K.S., Hodges, W.T., Bricker, D.K., Wisidagama, D.R., Compan, V., Remedi, M.S., Thummel, C.S., and Finck, B.N. (2016). An ancestral role for the mitochondrial pyruvate carrier in glucose-stimulated insulin secretion. *Mol. Metab.* 5, 602–614. <https://doi.org/10.1016/j.molmet.2016.06.016>.
- Vacanti, N., Divakaruni, A., Green, C., Parker, S., Henry, R., Ciaraldi, T., Murphy, A., and Metallo, C. (2014). Regulation of substrate utilization by the mitochondrial pyruvate carrier. *Mol. Cell* 56, 425–435. <https://doi.org/10.1016/j.molcel.2014.09.024>.
- Rumala, C.Z., Liu, J., Locasale, J.W., Corkey, B.E., Deeney, J.T., and Rameh, L.E. (2020). Exposure of pancreatic beta-cells to excess glucose results in bimodal activation of mTORC1 and mTOR-dependent metabolic acceleration. *iScience* 23, 100858. <https://doi.org/10.1016/j.isci.2020.100858>.
- Rutter, G.A., Pullen, T.J., Hodson, D.J., and Martinez-Sanchez, A. (2015). Pancreatic beta-cell identity, glucose sensing and the control of insulin secretion. *Biochem. J.* 466, 203–218. <https://doi.org/10.1042/BJ20141384>.
- Rutti, S., Dusaulcy, R., Hansen, J.S., Howald, C., Dermitzakis, E.T., Pedersen, B.K., Pinget, M., Plomgaard, P., and Bouzakri, K. (2018). Angiogenin and Osteoprotegerin are type II muscle specific myokines protecting pancreatic beta-cells against proinflammatory cytokines. *Sci. Rep.* 8, 10072. <https://doi.org/10.1038/s41598-018-28117-2>.
- Saikia, M., Jobava, R., Parisien, M., Putnam, A., Krokowski, D., Gao, X.H., Guan, B.J., Yuan, Y., Jankowsky, E., Feng, Z., et al. (2014). Angiogenin-cleaved tRNA halves interact with cytochrome c, protecting cells from apoptosis during osmotic stress. *Mol. Cell Biol.* 34, 2450–2463. <https://doi.org/10.1128/mcb.00136-14>.
- Schorn, A.J., Gutbrod, M.J., Leblanc, C., and Martienssen, R. (2017). LTR-retrotransposon control by tRNA-derived small RNAs. *Cell* 170, 61–71.e11. <https://doi.org/10.1016/j.cell.2017.06.013>.
- Sharma, U., Conine, C.C., Shea, J.M., Boskovic, A., Derr, A.G., Bing, X.Y., Belleannée, C., Kucukural, A., Serra, R.W., Sun, F., et al. (2016). Biogenesis and function of tRNA fragments during sperm maturation and fertilization in mammals. *Science* 351, 391–396. <https://doi.org/10.1126/science.aad6780>.
- Stolovich-Rain, M., Enk, J., Vikesa, J., Nielsen, F., Glaser, B., Dor, Y., and Dor, Y. (2015). Weaning triggers a maturation step of pancreatic β cells. *Dev. Cell* 32, 535–545. <https://doi.org/10.1016/j.devcel.2015.01.002>.
- Szabat, M., Kalynyak, T.B., Lim, G.E., Chu, K.Y., Yang, Y.H., Asadi, A., Gage, B.K., Ao, Z., Warnock, G.L., Piret, J.M., et al. (2011). Musashi expression in β -cells coordinates insulin expression, apoptosis and proliferation in response to endoplasmic reticulum stress in diabetes. *Cell Death Dis.* 2, e232. <https://doi.org/10.1038/cddis.2011.119>.
- Talchai, C., Xuan, S., Lin, H., Accili, D., and Accili, D. (2012). Pancreatic β cell dedifferentiation as a mechanism of diabetic β cell failure. *Cell* 150, 1223–1234. <https://doi.org/10.1016/j.cell.2012.07.029>.
- Tao, E.-W., Wang, H.-L., Cheng, W.Y., Liu, Q.-Q., Chen, Y.-X., and Gao, Q.-Y. (2021). A specific tRNA half, 5[′]tRNA-His-GTG, responds to hypoxia via the HIF1 α /ANG axis and promotes colorectal cancer progression by regulating LATS2. *J. Exp. Clin. Cancer Res.* 40, 67. <https://doi.org/10.1186/s13046-021-01836-7>.
- Theys, N., Bouckenoghe, T., Ahn, M.T., Remacle, C., and Reusens, B. (2009). Maternal low-protein diet alters pancreatic islet mitochondrial function in a sex-specific manner in the adult rat. *Am. J. Physiol. Regul. Integr. Comp. Physiol.* 297, R1516–R1525. <https://doi.org/10.1152/ajpregu.00280.2009>.
- Tsukita, S., Yamada, T., Takahashi, K., Munakata, Y., Hosaka, S., Takahashi, H., Gao, J., Shirai, Y., Kodama, S., Asai, Y., et al. (2017). MicroRNAs 106b and 222 improve hyperglycemia in a mouse model of insulin-deficient diabetes via pancreatic β -cell proliferation. *EBioMedicine* 15, 163–172. <https://doi.org/10.1016/j.ebiom.2016.12.002>.
- Vigueira, P.A., McCommis, K.S., Schweitzer, G.G., Remedi, M.S., Chambers, K.T., Fu, X., McDonald, W.G., Cole, S.L., Colca, J.R., Kletzien, R.F., et al. (2014). Mitochondrial pyruvate carrier 2 hypomorphism in mice leads to defects in glucose-stimulated insulin secretion. *Cell Rep.* 7, 2042–2053. <https://doi.org/10.1016/j.celrep.2014.05.017>.
- Wang, B., Chandrasekera, P.C., and Pippin, J.J. (2014). Leptin- and leptin receptor-deficient rodent models: relevance for human type 2 diabetes. *Curr. Diabetes Rev.* 10, 131–145. <https://doi.org/10.2174/1573399810666140508121012>.
- Xavier, V.J., and Martinou, J.-C. (2021). RNA granules in the mitochondria and their organization under mitochondrial stresses. *Int. J. Mol. Sci.* 22, 9502. <https://doi.org/10.3390/ijms22179502>.
- Xie, Y., Yao, L., Yu, X., Ruan, Y., Li, Z., and Guo, J. (2020). Action mechanisms and research methods of tRNA-derived small RNAs. *Signal. Transduct. Targeted Ther.* 5, 109. <https://doi.org/10.1038/s41392-020-00217-4>.

STAR★METHODS

KEY RESOURCES TABLE

REAGENT or RESOURCE	SOURCE	IDENTIFIER
Antibodies		
Guinea pig anti-insulin 1:100	Dako	Cat# XA0564
Goat anti-guinea pig IgG Alexa Fluor 488 1:500	Thermo Fisher	Cat# A-11073; RRID:AB_2534117
Goat anti-guinea pig IgG Alexa Fluor 555 1:500	Thermo Fisher	Cat# A-21435; RRID:AB_2535856
Goat anti-mouse IgG (H + L) 1:10000	Jackson ImmunoResearch	Cat# 211-035-109; RRID:AB_2339150
Goat anti-mouse IgG Alexa Fluor 555 1:500	Thermo Fisher	Cat# A-21422; RRID:AB_2535844
Goat anti-rabbit IgG (H + L) 1:10000	Jackson ImmunoResearch	Cat# 115-035-003; RRID:AB_10015289
Goat anti-rabbit IgG Alexa Fluor 488 1:500	Thermo Fisher	Cat# A-11008; RRID:AB_143165
Mouse anti hnRNPA1 1:500	Santa Cruz Biotechnology	Cat# Sc-32301; RRID:AB_627729
Mouse anti-Akt 1: 500	Cell Signaling Technology	Cat# 2920; RRID:AB_1147620
Mouse anti-Beta-actin 1:2000	Santa Cruz Biotechnology	Cat# Sc-47778; RRID:AB_626632
Mouse anti-BrdU 1:400	BD Biosciences	Cat# BD55627
Mouse anti-glucagon 1:1000	Abcam	Cat# Ab10988; RRID:AB_297642
Mouse anti-Msi1 (WB) 1:500	Santa Cruz Biotechnology	Cat# Sc-135721; RRID:AB_10610465
Mouse anti-Tubulin 1:2000	Sigma	Cat# T5168; RRID:AB_477579
Rabbit anti-calreticulin 1:100	Homemade	N/A
Rabbit anti-Caprin1 1:200	Proteintech	Cat# 15112-1-AP; RRID:AB_2070016
Rabbit anti-Cox IV 1:500	Cell Signaling Technology	Cat# 4850; RRID:AB_2085424
Rabbit anti-Ki67 1:700	Abcam	Cat# Ab15580; RRID:AB_443209
Rabbit anti-MPC1 1:1000	Cell Signaling Technology	Cat# 14462; RRID:AB_2773729
Rabbit anti-Mrpl38 1:200	Proteintech	Cat# 15913-1-AP; RRID:AB_2146047
Rabbit anti-Msi1 (ICC) 1:200	Sigma	Cat# AB5977
Rabbit anti-p-Akt 1:500	Cell Signaling Technology	Cat# 4060; RRID:AB_2315049
Rabbit anti-Survivin 1:1000	Abcam	Cat# Ab182132
Chemicals, peptides, and recombinant proteins		
BrdU	Abcam	Cat# Ab142567
Hoechst 33342	Invitrogen	Cat# H21492
IFN γ	R&D system	Cat# 485-MI
IL-1 β	Peptotech	Cat# 211-11B
M-280 Streptavidin Dynabeads	Invitrogen	Cat# 11206D
Mitotracker Deep Red FM	Thermo Fisher	Cat# M22426
TNF α	Peptotech	Cat# 315-01A
UK5099	Sigma	Cat# PZ0160
Critical commercial assays		
Imprint RNA Immunoprecipitation Kit	Sigma	RIP-12RXN
rtStar tRF&tiRNA Pretreatment Kit	Arraystar	Cat# AS-FS-005
Seahorse XFp Cell Mito Stress Test Kit	Agilent	Cat# 103010-100
TUNEL In Situ Cell Death Detection Kit	Sigma	Cat# 11684795910
Deposited data		
P10 vs adult rat islet tRF profiling	This paper	GEO: GSE163582
P10 rat islet RNA-seq upon tiRNA-5 inhibition	This paper	GEO: GSE163584
Experimental models: Cell lines		
INS832/13 cell line	Dr. C. Newgard	Hohmeier et al., 2000

(Continued on next page)

Continued

REAGENT or RESOURCE	SOURCE	IDENTIFIER
Experimental models: Organisms/strains		
Sprague Dawley Rats	Janvier	RjHan:SD
Oligonucleotides		
Angiogenin SMARTpool siRNA	Dharmacon	Cat# L-086613-02
miRCURY LNA inhibitor Control (Neg A)	Qiagen	Cat# 339126
miRCURY LNA inhibitors customized	Qiagen	Cat# 339121
Mpc1 SMARTpool siRNA	Dharmacon	Cat# L-093029-02
Msi1 SMARTpool siRNA	Dharmacon	Cat# L-097920-02
Nontargeting SMARTpool siRNA	Dharmacon	Cat# D-001810-10
Software and algorithms		
RStudio 2022.02.1	RStudio	https://www.rstudio.com
GraphPad Prism 8	GraphPad	https://www.graphpad.com
BioRender Illustration Tool 2022	BioRender	https://app.biorender.com/

RESOURCE AVAILABILITY

Lead contact

Further information and requests for resources and reagents may be directed to and will be fulfilled by the Lead Contact, Romano Regazzi (romano.regazzi@unil.ch).

Materials availability

No new unique reagents were generated in this study.

Data and code availability

RNA-seq data were deposited at GEO and are publicly available. Accession numbers are provided in the [Key resources table](#). No unique codes were generated in this study. Any additional information required to reanalyze data presented in this study can be requested from the [Lead Contact](#).

EXPERIMENTAL MODEL AND SUBJECT DETAILS

Ethical statement

All procedures were performed in agreement with the NIH guidelines and approved by the Swiss federal food safety and veterinary offices.

Rats

Three-month-old adult male Sprague-Dawley rats and three-month-old pregnant Sprague-Dawley rats were purchased from Janvier Laboratories (Le Genest-Saint-Isle, France). Rat pups were collected at postnatal day 10 (P10). For the low protein (LP) diet model, Sprague-Dawley female rats were fed either a control diet (16.1% [w/w] protein, U8978P Version 0022, Safe-diet, France) or an LP diet (5% [w/w] protein, U8959P Version 0156, Safe-diet, France) during pregnancy and lactation. Animals were housed under standard conditions on a 12h light/dark cycle with free access to chow or LP diet and water. Islet RNA samples from C57BL/KsJ db/db and C57BL/6J ob/ob mice (13–16 weeks old) and age-matched lean control mice (db/+ C57BL/KsJ and –/– C57BL/6J, respectively) were kindly provided by Dr D. Ross Laybutt (Australia).

METHOD DETAILS

Pancreatic islet isolation and culture

Rat pancreatic islets were isolated using collagenase P (Sigma, #11213865001) digestion, histopaque density gradient (Sigma, 1077 and 1119) and handpicking (Gotoh et al., 1987). P10 rat pancreata were harvested and digested in collagenase by handshaking for 5 min. Isolated islets were recovered in RPMI 1640 GlutaMAX medium (Invitrogen) containing 11 mM glucose and 2 mM L-glutamine and supplemented with 10% fetal calf serum (Sigma), 10 mM Hepes pH 7.4, 1 mM sodium pyruvate, 100 µg/mL streptomycin and 100 IU/mL penicillin before being dissociated into single cells by incubation in Ca²⁺/Mg²⁺ free phosphate buffered saline, 3 mM EGTA and 0.002% trypsin for 3.5 min at 37°C.

Enriched fractions of α - and β -cells were obtained by Fluorescence-Activated Cell Sorting (FACS) of dissociated islet cells based on β -cell autofluorescence as previously described (Guay et al., 2019). FACS purity was evaluated by double immunofluorescence using mouse anti-glucagon and guinea pig anti-insulin antibodies. β -cell fractions contained $99.1 \pm 0.9\%$ insulin-positive cells and $0.6 \pm 0.6\%$ glucagon-positive cells, while α -cell-enriched fractions contained $10.6 \pm 8.2\%$ insulin-positive cells and $88.8 \pm 8.2\%$ glucagon-positive cells.

Cell culture

INS832/13 rat β -cell line, provided by Dr. C. Newgard (Duke University) (Hohmeier et al., 2000), was cultured in RPMI 1640 GlutaMAX medium (Invitrogen) containing 11 mM glucose and 2 mM L-glutamine and supplemented with 10% fetal calf serum (Sigma), 10 mM HEPES pH 7.4, 1 mM sodium pyruvate and 0.05 mM of β -mercaptoethanol. INS832/13 cells were cultured at 37°C in a humidified atmosphere (5% CO₂, 95% air) and tested negative for mycoplasma contamination.

Small RNA-sequencing

RNA was isolated from pancreatic islets of three adult male rats and three independent P10 litters using miRNeasy micro kit (QIAGEN). Small RNA-sequencing, tRF annotation and data analyses were performed by Arraystar (Rockville, MD, USA). For efficient reverse transcription, the following treatments were done by Arraystar on RNA samples prior to sequencing library construction: 3'-aminoacyl (charged) deacylation to 3'-OH for 3' adaptor ligation, 3'-cP (2',3'-cyclic phosphate) removal to 3'-OH for 3' adaptor ligation, 5'-OH (hydroxyl group) phosphorylation to 5'-P for 5'-adaptor ligation, m1A and m3C demethylation. Sequencing libraries were size-selected for the RNA biotypes to be sequenced using an automated gel cutter. The libraries were qualified and absolutely quantified using Agilent BioAnalyzer 2100 and sequenced using Illumina NextSeq 500. For small RNA sequencing, the sequencing type was 51-bp single-read at 10M reads. Image analysis and base calling were performed using Solexa pipeline v1.8 (OffLine Base Caller software, v1.8). Sequencing quality was examined by FastQC software and trimmed reads (pass Illumina quality filter, trimmed 3'-adaptor bases by cutadapt) were aligned to mature-tRNA and pre-tRNA sequences from GtRNAdb using NovoAlign software (v2.07.11). The remaining reads were aligned to the transcriptome sequences (mRNA/rRNA/snRNA/snoRNA/piRNA/miRNA). The expression profiling and differential expression of tRFs, tiRNAs and known miRNAs were calculated based on normalized TPM. Hierarchical clustering, scatterplots and volcano plots were performed with the differentially expressed tRFs and tiRNAs in R or Python environment for statistical computing and graphics.

tRF quantification

To remove tRNA-modifications that may interfere with the quantification of tRNA-derived fragments, RNA was pretreated with rtStarTM tRF&tiRNA Pretreatment Kit (Arraystar). Real-time PCR quantification of tRNA-derived fragments was performed using the miRCURY LNA Universal RT microRNA PCR system (QIAGEN). The input sequences used for primer design are indicated in Table S3.

Inhibition of tRFs

Dispersed islet cells of P10 rats were transfected with 20 picomole tRF or scrambled control inhibitor for 72h using Lipofectamine 2000 (Invitrogen).

siRNA treatment

Dispersed islet cells of P10 rats or INS832/13 cells were transfected with 40 picomole siRNAs for 72h with the use of Lipofectamine (2000) (Invitrogen).

Immunocytochemistry

Transfected cells on coverslips were fixed with methanol, permeabilized with saponin (0.5% in PBS), and blocked with 1% BSA. The coverslips were incubated with the primary antibodies for 1h at room temperature, and secondary antibodies for 30 min at 37°C. Hoechst 33342 was used to visualize cell nuclei. For BrdU incorporation, cells were incubated with BrdU for 48h. For TUNEL assay, DNA was denatured with 2N HCl. Images were obtained with Zeiss AxioVision. Mitochondria of INS832/13 cells were labeled with MitoTrackerTM for 15 min at a 200 nM concentration.

Insulin secretion and insulin ELISA

For insulin secretion, transfected islet cells were washed and incubated at 37°C for 1h in KREBS Buffer (25 mM HEPES, pH 7.4, 0.1% BSA, and 2 mM glucose). The cells were sequentially incubated at 37°C for 1h in KREBS supplemented with 2 mM glucose (basal) or 10 mM glucose and 1 mM L-leucine (stimulatory) and supernatants were collected. The cells were harvested in acidic ethanol (75% ethanol, 0.55% HCl) or RIPA buffer (Thermo Scientific) to determine cellular insulin and protein content, respectively. Insulin levels were measured by ELISA (Mercodia) and protein concentration by Bradford assay (Thermo Fisher).

RNA sequencing

RNA from transfected P10 Sprague Dawley islet cells ($n = 4$ per condition) were extracted with miRNeasy Micro kit (QIAGEN). Library preparation, sequencing, and data processing were conducted by Lausanne Genomic Technologies Facility. Sequencing libraries

were prepared with the TruSeq Stranded mRNA Library Prep kit and a HiSeq 2500 instrument for a single end run of 125 cycles using the SBS chemistry v4 (Illumina). For data processing, adaptors and low-quality bases were trimmed from raw sequencing reads using CutAdapt (Version 1.8) and FASTX-Toolkit (Version 0.0.13.2) and reads less than 16nt were discarded. After quality control and data filtering, reads were aligned to the reference genome Rnor_6.0 by TopHat2 (v2.1.1), allowing 3 mismatches. Reads only unambiguously aligned were preserved to calculate reads number and RPKM value (RPKM represents reads per kilobase and per million) for each gene. Differentially expressed genes between the paired groups were analyzed by using edgeR in R packages. The genes were retained for further analysis if their expression reached count-per-million levels above 1 in at least 1 sample. For each gene, significance p value was obtained based on the model of negative binomial distribution. Fold changes of gene expression were also estimated within the edgeR statistical package. The criterion for DEG has been set as fold change >2 and $p < 0.05$.

Protein digestion for mass spectrometry

Frozen pellets of transfected (72h) dispersed islet cells of P10 rats ($n = 4$) were digested with a modified version of the iST method (Kulak et al., 2014), and analyzed by Liquid Chromatography-tandem Mass spectrometry. The frozen pellets were resuspended in 50 μ L miST lysis buffer (1% Sodium deoxycholate, 100 mM Tris pH 8.6, 10 mM DTT) by vigorous vortexing. Resuspended samples were heated at 95°C for 5 min and protein concentration was determined by the tryptophane fluorescence method. Samples were then diluted 1:1 (v:v) with water containing 4 mM MgCl₂ and Benzonase (Merck #70746, 2,5 Units/ μ L) and incubated for 15 min at RT to digest nucleic acids. Reduced disulfides were alkylated by adding ¼ vol (25 μ L) of 160 mM chloroacetamide (final concentration of 32 mM) and incubated at 25°C for 45 min in the dark. Samples were adjusted to 3 mM EDTA and digested with 0.5 μ g Trypsin/LysC mix (Promega #V5073) for 1h at 37°C, followed by a second 1h digestion with an identical aliquot of proteases. To remove sodium deoxycholate, two sample volumes of isopropanol containing 1% TFA were added to the digests, and the samples were desalted on a strong cation exchange (SCX) plate (Oasis MCX; Waters Corp., Milford, MA) by centrifugation. After washing with isopropanol/1% TFA, peptides were eluted in 250 μ L of 80% MeCN, 19% water, 1% (v/v) ammonia.

Liquid Chromatography-tandem mass spectrometry (LC-MS)

Eluates after SCX desalting were dried, and resuspended in variable volumes of 0.05% trifluoroacetic acid, 2% acetonitrile to equilibrate concentrations. A total of 1 μ g of each sample was injected on a column for nanoLC-MS analysis.

MS analysis

Data-dependent LC-MS/MS analysis of TMT sample was carried out on a Fusion Tribrid Orbitrap mass spectrometer (Thermo Fisher Scientific) interfaced through a nano-electrospray ion source to an Ultimate 3000 RSLCnano HPLC system (Dionex). Peptides were separated on a reversed-phase custom packed 40 cm C18 column (75 μ m ID, 100 \AA , Reprosil Pur 1.9 μ m particles, Dr. Maisch, Germany) with a 4–76% acetonitrile gradient in 0.1% formic acid (total time 140 min). Full MS survey scans were performed at 120'000 resolution. A data-dependent acquisition method controlled by Xcalibur 4.2 software (Thermo Fisher Scientific) was used that optimized the number of precursors selected ("top speed") of charge 2 + to 5 + while maintaining a fixed scan cycle of 1.5s. The precursor isolation window used was 0.7 Th. Full survey scans were performed at a 120'000 resolution, and a top speed precursor selection strategy was applied to maximize acquisition of peptide tandem MS spectra with a maximum cycle time of 0.6s. HCD fragmentation mode was used at a normalized collision energy of 32%, with a precursor isolation window of 1.6 m/z, and MS/MS spectra were acquired in the ion trap. Peptides selected for MS/MS were excluded from further fragmentation during 60s.

Western blotting

Proteins were extracted from transfected P10 islet cells using RIPA buffer (Thermo Fisher) and quantified by Bradford Assay (Thermo Fisher). A total of 10 μ g of protein was loaded on SDS-PAGE and transferred to a nitrocellulose membrane (Bio-RAD). Membranes were blocked in 5% BSA (Sigma) in TBS-T and incubated overnight at 4°C with the primary antibody, and for 1h at RT with the secondary antibody. ECL substrate (Pierce, #32106) was used to reveal the membranes.

Mitochondrial fractionation

Mitochondria were isolated from 2×10^6 INS832/13 cells as previously described (Lampl et al., 2015), with some modifications. Cells were collected, washed 3 times with PBS and resuspended in 1 mL of ice-cold mitochondrial isolation buffer (MIB: 200mM sucrose, 10mM Tris/MOPS, 1mM EGTA/Tris, pH 7.4; 1M Tris/MOPS: 12.1g of Tris base in 70mL H₂O, MOPS added to get pH 7.4, final volume adjusted to 100mL with water, filter sterilized and store at +4°C; 0.2 M EGTA/Tris: 3.8 g of EGTA to 10 mL of H₂O, ~30–40 mL of 1 M Tris/MOPS added until it dissolved, final volume adjusted to 50 mL with water, solution filtered and stored at room temperature (the pH will be ~6.7). The cells were sonicated for 3 times 15 s. The solution was drawn into a 1 mL syringe using a 27 gauge needle and thrown it out back into the 1.5mL tube by expelling it against the inside wall of the tube in order to use that force to further break out cell membrane. This syringe step was repeated 3 times. The samples were then centrifuged for 5 min at 600 x g, 4°C. The supernatant was collected and centrifuged at 10,000 x g, 4°C for 5 min. The pellet containing the mitochondria was resuspended in 700 μ L of Trizol, left on ice for 5 min and vortexed for 30 s before RNA isolation using miRNeasy micro kit (QIAGEN).

Mitochondrial respiration

Oxygen consumption rates (OCRs) of dispersed and transfected islet cells from P10 Sprague Dawley rats were analyzed with XFp Extracellular Flux Analyzer (Agilent Technologies). Prior to analysis, cells were starved in KREBS solution (114 mM NaCl, 4.7 mM KCl, 1.2 mM KH_2PO_4 , 1.16 mM MgSO_4 , 2.5 mM $\text{CaCl}_2 \cdot 2\text{H}_2\text{O}$, 20 mM HEPES, pH 7.4) supplemented with 2 mM glucose and 0.2% BSA for 1 h at 37°C without CO_2 . To block Mpc-complex, an additional 150 μM UK5099 in DMSO was supplemented to the KREBS solution. Mitochondrial respiration was measured at basal (2 mM) glucose followed by subsequent injections of 20 mM glucose/1 mM L-leucine, 5 μM oligomycin, 2 μM FCCP, and 1 μM rotenone/1 μM antimycin A. Data were normalized to protein content. Basal respiration was calculated by subtracting non-mitochondrial respiration (minimum rate after rotenone/antimycin A injection) from the last measurement before oligomycin injection, maximal respiration by subtracting non-mitochondrial respiration from the first measurement after FCCP injection, response to glucose and L-leucine by subtracting the last measurement of basal respiration from the last measurement after glucose/L-leucine injection, ATP production by subtracting the minimum measurement after oligomycin injection from the last basal measurement, and coupling efficiency by dividing ATP production by basal respiration.

Identification of tRNA-5^{HisGTG} interacting proteins

tRNA-5^{HisGTG} interacting proteins were identified as previously reported (Krishna et al., 2019), with some modifications. Potential Mpc1-tRNA-5 interactions were investigated with an RNA immunoprecipitation kit (Imprint Kit, RIP-12RXN, Sigma). First, protein Agarose A beads were coupled to 5 μg of either MPC1 or IgG antibody. INS832/13 cell lysates (5×10^6 cells per condition) were prepared in a hypotonic lysis buffer that preserves RNA-protein interactions (Imprint Kit, RIP-12RXN, Sigma). Then, the antibody-treated beads were incubated with the INS832/13 cells lysates overnight at 4°C. Beads were washed thoroughly, and equal volumes were used for Western blot and qPCR analyses. For Western blot analysis, immunoprecipitated proteins were eluted by boiling the beads in 2x Laemmli buffer (Bio-Rad). MPC1 and IgG immunoprecipitated samples, as well as a cell lysate input (10%), was run on a 4–15% SDS-PAGE gel. MPC1 immunoprecipitation was confirmed by blotting the nitrocellulose membrane with MPC1 antibody as previously described. For real-time PCR analysis, Qiazol reagent (QIAGEN) was added directly on to beads and small RNAs were extracted with RNeasy micro kit (QIAGEN). tRNA-derived fragments were then quantified by as previously described.

tRNA-5^{HisGTG} pull-down and Mass Spectrometry

A total of 3 μg of 3'-biotinylated oligonucleotides mimicking the sequence of tRNA-5^{HisGTG} or its scrambled control is heated at 95°C for 2 min, recovered on ice for 2 min, and refolded at room temperature for 20 min in 100 μl of RNA structure buffer (10 mM Tris pH 7.0, 0.1 M KCl, 10 mM MgCl_2). The refolded oligonucleotides are incubated at room temperature for 1 h (rotating) with 1 mg of INS832/13 cell lysate prepared with a harsh lysis solution (50 mM Tris-HCl pH 7.5, 150 mM NaCl, 1% NP40, 0.1% SDS, 0.5% sodium deoxycholate, 1 mM DTT, protease inhibitor cocktail, 80 U/ml RNase inhibitor). The samples are then incubated with 50 μL of streptavidin dynabeads (M-280 Streptavidin, 11206D, Invitrogen) for another 1 h at room temperature. The beads are washed thoroughly (50 mM Tris-HCl pH 7.5, 150 mM NaCl, 1% NP40, 0.1% SDS, 0.5% sodium deoxycholate), and the proteins are eluted by heating the samples in Laemmli buffer at 95°C for 5 min. Washed beads were eluted in 25 μl of elution buffer (5% SDS, 50 mM Triethylammonium bicarbonate (TEAB), 5 mM tricarboxyethylphosphine, 30 mM chloroacetamide, pH 8.5) by heating at 95°C for 5 min under agitation. The supernatant was collected and subjected to trypsin digestion according to the S-TRAP (Protifi, Farmingdale, NY) method. Briefly, an aliquot of 12% phosphoric acid was added to lower pH to 3.0, followed by dilution with 4 volumes of S-TRAP loading buffer (100 mM (final concentration) TEAB pH 8.0, in 90% MeOH). The obtained mixture was passed by centrifugation on S-TRAP micro cartridges, which were then washed 3 times with 600 μl of loading buffer. Digestion was started by adding to the cartridges 2 μg of Trypsin (Promega) in 25 μL of 50 mM TEAB, pH 8 and was carried out for 2 h at 47°C without shaking. Digested peptides were eluted by centrifugation, followed by further elution of the cartridge with 40 μL of 50 mM TEAB, then 40 μl of 0.2 formic acid and 40 μl of 50% acetonitrile (each time at 3000 x g for 1 min). All eluates were pooled and dried by evaporation.

Tryptic peptide mixtures (5 μl) were resuspended in 2% acetonitrile, 0.05% TFA and injected on a Dionex RSLC 3000 nanoHPLC system (Dionex, Sunnyvale, CA, USA) interfaced via a nanospray source to a high resolution QExactive Plus mass spectrometer (Thermo Fisher Scientific). Peptides were separated on an Easy Spray C18 PepMap nanocolumn (25 or 50 cm x 75 μm ID, 2 μm , 100Å, Dionex) using a 110 min gradient from 2 to 90% acetonitrile in 0.1% formic acid for peptide separation. Full MS survey scans were performed at 70,000 resolution. In data-dependent acquisition controlled by Xcalibur software (Thermo Fisher), the 10 most intense multiply charged precursor ions detected in the full MS survey scan were selected for higher energy collision-induced dissociation (HCD, normalized collision energy NCE = 27%) and analysis in the orbitrap at 17,500 resolution. The window for precursor isolation was of 1.6 m/z units around the precursor and selected fragments were excluded for 60 s from further analysis.

Tandem MS data were processed by the MaxQuant software (version 1.6.3.4) incorporating the Andromeda search engine. The UniProt Rattus norvegicus reference proteome (RefProt) database of January 2019 was used (29,959 sequences), supplemented with sequences of common contaminants. Trypsin (cleavage at K, R) was used as the enzyme definition, allowing 2 missed cleavages. Carbamidomethylation of cysteine was specified as a fixed modification. N-terminal acetylation of protein and oxidation of methionine were specified as variable modifications. The match between runs function was not activated. All identifications were filtered at 1% FDR at both the peptide and protein levels with default MaxQuant parameters.

QUANTIFICATION AND STATISTICAL ANALYSIS

Data are represented as mean \pm standard deviation. Statistical analyses were conducted using GraphPad Prism 8. Plots and figures were prepared on RStudio and GraphPad Prism 8. A two-tailed one-sample t test was used to compare data when control was set to 1. A two-tailed t test was used when comparing two datasets. ANOVA was used to compare multiple datasets, followed by Tukey, Dunnett, or GamesHowell post hoc tests. Correlation of datasets was assessed by a two-tailed Pearson test. Differences between datasets were considered statistically significant when p values <0.05 .